



PAPER

Finite locally resonant metafoundations for the protection of slender storage tanks against vertical ground accelerations

To cite this article: Andrea Franchini *et al* 2020 *Smart Mater. Struct.* **29** 055017

View the [article online](#) for updates and enhancements.

Finite locally resonant metafoundations for the protection of slender storage tanks against vertical ground accelerations

Andrea Franchini¹ , Oreste S Bursi¹ , Francesco Basone² and Feifei Sun³

¹ University of Trento, Via Mesiano 77, I-38123, Trento, Italy

² Engineering and Architecture Faculty, University of Enna 'Kore', Viale delle Olimpiadi, I-94100 Enna, Italy

³ State Key Laboratory of Disaster Reduction in Civil Engineering, Tongji University, 1239 Siping Road, 200092 Shanghai, People's Republic of China

E-mail: oreste.bursi@unitn.it

Received 22 September 2019, revised 16 February 2020

Accepted for publication 9 March 2020

Published 31 March 2020



CrossMark

Abstract

Inspired by recent findings in the field of Metamaterials, finite lattice locally resonant metafoundations represent an innovative solution for the seismic protection of storage tanks. One of the advantages with respect to traditional rubber bearings is the possibility of protecting the structure against the vertical component of ground accelerations, which has a significant influence on the hydrodynamic pressure of tanks. In this respect, we propose feasible configurations for a finite lattice metafoundation formed by steel columns, concrete slabs and concrete resonators, which allow for the protection of a slender tank against earthquakes with a significant vertical component. Based on the acceleration response variance of the liquid mass involved in the breathing mode, we develop an optimization procedure in frequency domain, which is adopted to design resonators stiffness and damping ratio. Time history analyses validate the efficacy of the proposed systems and show that staggering the columns at the second level of the outer frame allows for a higher attenuation of base pressure; it can decrease by 22.7% and 23.3% for OBE and SSE earthquakes, respectively. Eventually, we investigate the relationships between seismic signals frequency content and dynamic properties of coupled foundation-tank systems.

Keywords: earthquake engineering, seismic isolation, finite locally resonant metafoundation, vertical accelerations, liquid storage tanks

(Some figures may appear in colour only in the online journal)

1. Introduction

1.1. Background and motivation

During the Kocaeli earthquake—Turkey, 1999, $M_w = 7.4$, the majority of the tanks of Tupras refinery, which accounted for one third of Turkey's oil production, was made inactive due to buckling of tank walls, poor performance of floating roof systems and fire related damages [1]. Through the analysis of this event and other case histories, Krausmann *et al* [2] showed that pipes and storage tanks were the most

vulnerable equipment when subjected to floods, lightning and seismic events. A possible approach for the seismic protection of storage tanks consists in base isolation through rubber bearings. However, the main problem of this solution is the significant residual horizontal displacement after earthquake. Moreover, although base isolation technology is efficient in the horizontal direction, little can be done against the vertical component of ground accelerations [3]. With regard to tank protection, the vertical component entails additional hydrodynamic pressure on tank walls [4]. This additional contribution is uniformly distributed in the circumferential direction;

and with a peak ground acceleration (PGA) of about $1/3 g$ [5], it could reach the level of hydrostatic effects. High PGA is common for near-field records of strong earthquakes [6]. Hence, isolation in vertical direction is quite important for tanks.

Recently, locally resonant metafoundations are proposed as an innovative approach for base isolation. Hereinafter, they are referred to as ‘metafoundations’ or simply ‘foundations’. The system consists in the periodic arrangement of local resonators, and is inspired by researches in the field of metamaterials and phononic crystals. Such a configuration is able to attenuate or forbid elastic waves propagation within selected ranges of frequencies, which are called attenuation zones or band gaps. Locally resonant periodic crystals were proposed by Liu *et al* [7]; they realized three-component composites consisting of hard spheres coated with a soft cladding and dispersed in a stiff host medium. By taking advantage of resonators which can store and transfer energy, band gaps with lattice constants of several orders of magnitude smaller than mechanical wavelengths were realized. Based on the aforementioned and other researches, Jia and Shi [8] proposed metafoundations to isolate structures against seismic waves. Their metafoundation consists of unit cells which are formed of steel cylinders coated by rubber and embedded in a concrete matrix; it was applied for the isolation of a six-story building. Xiang *et al* [9] analyzed a 1D layered metafoundation formed by the periodic overlapping of strata of two different materials. Shi and Huang [10] studied a 3D three-component metafoundation whose unit cell was formed of a high-density core, a soft coating and a concrete matrix. They realized a linear elastic soil-foundation FE model and showed the efficacy of the foundation in reducing the acceleration response of a reference point on its surface. In order to compare the Bragg-scattering and local resonance band gap generation mechanism, Cheng and Shi [11] examined periodic structures with two- and three-component inclusions. They showed the efficacy of the proposed systems for the protection of a nuclear reactor, which was modeled as a SDoF lumped mass. Field experiments of scaled 2D and 3D metafoundations were presented in [12, 13]. Relevant experiments showed the efficacy in seismic mitigation of metafoundations and the accuracy of FE models for their characterization. In order to study the influence of torsional movement on the band gap mechanism, Huang *et al* [14] proposed a metafoundation composed of a concrete matrix endowed with steel cylinders connected with rubber linkers. A metafoundation operating in both horizontal and vertical directions was proposed by Cheng and Shi [15]. Since the frequency content of a seismic event in the horizontal direction is different from that in the vertical one, the authors proposed to implement two types of unit cells. Each unit cell targets to realize the isolation in one direction. The efficacy of the foundation was evaluated by comparing the response spectra of SDoF systems subjected to filtered and not-filtered ground motions. Casablanca *et al* [16] studied a foundation composed of concrete plates with embedded cylindrical steel resonators and experimentally proved its efficacy against harmonic excitations. La Salandra *et al* [17] proposed a metafoundation

whose unit cell was formed of concrete columns, concrete slabs and concrete resonators connected by means of steel springs; the system was applied to protect a broad storage tank against the horizontal components of ground motion. The authors also proved that the coupling between tank and foundation modifies the band gap frequency range. In order to improve the flexibility of the foundation, Basone *et al* [18] substituted concrete columns with steel ones. The system was applied for the protection of a slender and a broad fuel storage tank. The foundation was designed according to the Italian standards [19] and resonators were optimized in frequency domain, taking the feedback of the superstructure into account. Time history analyses proved the efficacy of the metafoundation in the reduction of base shear; moreover, they showed that a higher attenuation can be achieved by reducing the shear stiffness of the foundation outer frame. Through research on 1D metamaterials, Geng *et al* [20] showed that a low global stiffness of the metamaterial was required for the isolation against low frequency seismic waves; such a requirement may prevent the use of locally resonant metamaterials as underlying foundations against the vertical component of earthquakes.

In addition to metafoundations, a significant number of seismic isolation devices and approaches inspired by periodicity and local resonance have been proposed in recent years. For instance, Palermo *et al* [21] analyzed a seismic metabarrier consisting of soil-embedded surface resonators, which were used to redirect the surface waves into the bulk. To enlarge band gaps generated by this system, the possibility of using multi-mass resonators was investigated in [22]. Eventually, in order to analyze the wave dispersion properties of multi-story buildings, Cheng *et al* [23] applied periodic structures theory. They calculated the band gap generated by the structure and showed that if the main frequency of the seismic record was in the band gap, the upper structure response would decrease.

In the literature, there is a lack of analytical models for fluid-tank interaction subjected to both horizontal and vertical seismic excitation; thus, the analysis of a 3D metafoundation performance subjected to both horizontal and vertical ground motions requires a finite element high-fidelity model of the coupled metafoundation-superstructure system. Since the efficacy of a framed metafoundation against horizontal ground shakings was already investigated by two of the authors by means of analytical models [18, 24], the aforementioned metafoundations subjected to vertical components of ground acceleration are further explored hereinafter.

1.2. Scope

Along these lines, the aim of this study is to propose feasible and efficient configurations which allow an enhancement of metafoundations suggested by Basone *et al* [18] for vertical components of ground acceleration. Thus, to crystallize ideas, we consider a slender tank as a case study for superstructure. Therefore: (i) in order to isolate the prototype tank in the vertical direction, we propose and study different metafoundations singled out by number of layers, columns height

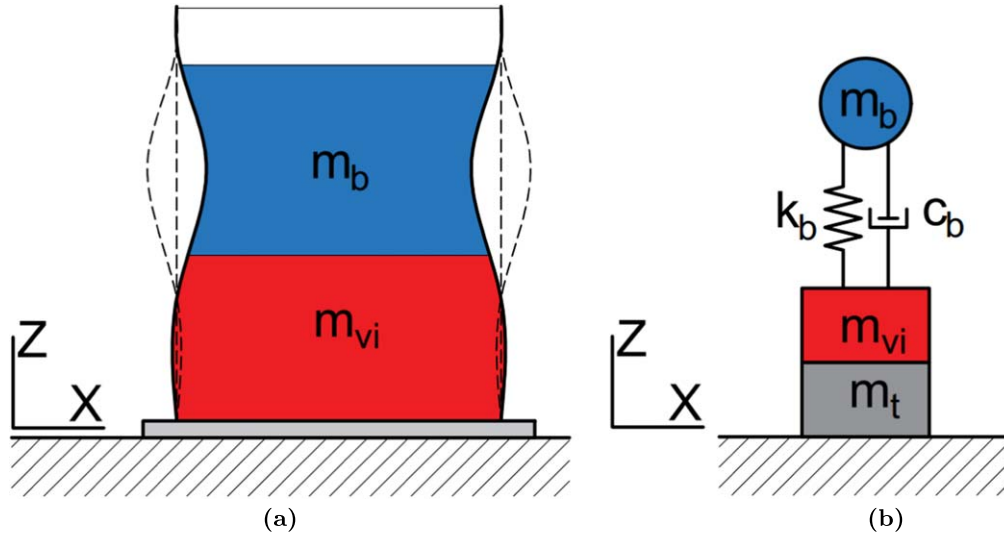


Figure 1. Vertical dynamic behavior of a liquid-filled storage tank. (a) Breathing mode of vibration; (b) lumped mass model proposed in [5].

and columns arrangement; (ii) to increase the flexibility of the foundation system, we propose the staggering of columns at the second level of the foundation; (iii) in order to reduce the hydrodynamic base pressure, we optimize the stiffness and damping of resonators in the vertical direction, considering the effects of foundation-tank interaction; (iv) to single out the systems that are not efficient in controlling the superstructure response, we investigate the spectral properties of ground motions.

The remainder of the article is organized as follows. Section 2 describes the proposed metafoundations, the dynamic model used to study the behavior of the coupled foundation-tank system, the accelerograms selection and the foundation seismic design. Section 3 introduces considerations on metamaterials and periodic lattice concepts. Based on stochastic stationary process theory, resonators parameters are optimized in section 4. Moreover, in section 5, we evaluate the performance of the optimized structures subjected to natural seismic records. Eventually, we draw conclusions and present future developments in section 6.

2. Description of the coupled foundation-tank system

2.1. Liquid storage tank modeling

In a liquid-filled storage tank, the vertical component of ground acceleration induces additional horizontal hydrodynamic pressure which increases the hoop stress in the wall. The hydrodynamic pressure acting on the wall can be divided into three contributions [25]:

$$p_v(t) = p_{vs}(t) + p_{vi}(t) + p_{vb}(t). \quad (1)$$

More precisely: p_{vs} is the long-period component deriving from the convective fluid motion, also known as sloshing; p_{vi} is the impulsive fluid pressure component which varies in synchronism with the vertical ground acceleration; p_{vb} the

short-period component, derives from the tank walls radial, axisymmetric vibration, which is called breathing mode. As shown in figure 1(a), it consists of successive radial expansions and contractions.

Experimental studies showed that the sloshing contribution is negligible when induced by transient vertical motion [25]. Neglecting the sloshing mass, Veletsos and Tang [5] proposed a two-mass mechanical analogy to represent the tank-liquid system and evaluate vertical earthquake-induced impulsive and breathing pressures. According to this model, depicted in figure 1(b), a portion of the liquid mass m_l , corresponding to impulsive mode and denoted as m_{vi} , is rigidly linked to the tank base; the remaining mass, corresponding to breathing mode and denoted as m_b , is flexibly connected through a spring k_b . The breathing mass can be calculated as $m_b = m_l \cdot \alpha_m$, where α_m is a nondimensional factor, tabulated as a function of the tank slenderness (ratio H/R of liquid height to tank radius). The natural frequency of the breathing mode is obtained as $\omega_b = \omega_0 \cdot \alpha_\omega$, where α_ω is tabulated as a function of the tank slenderness and

$$\omega_0 = \frac{1}{R} \sqrt{\frac{E_t}{\rho_t}} \quad (2)$$

is the natural frequency of the breathing mode for a ring with same cross section as the tank wall. E_t and ρ_t are the tank material elastic modulus and density, respectively. The values of $\alpha_m = m_b/m_l$ and $\alpha_\omega = \omega_b/\omega_0$ suggested in [5] are plotted against H/R in figure 2. Eventually, the breathing stiffness is calculated as:

$$k_b = m_b \cdot \omega_b^2. \quad (3)$$

The impulsive mass is calculated by $m_{vi} = m_l - m_b$. The tank mass m_t is assumed as rigidly attached to m_{vi} . The properties of the considered tank, which is located in the refinery of Priolo Gargallo (Italy), are shown in table 1. The viscous coefficient is taken as $c_b = 2\xi k_b \omega_b$, where $\xi = 0.005$.

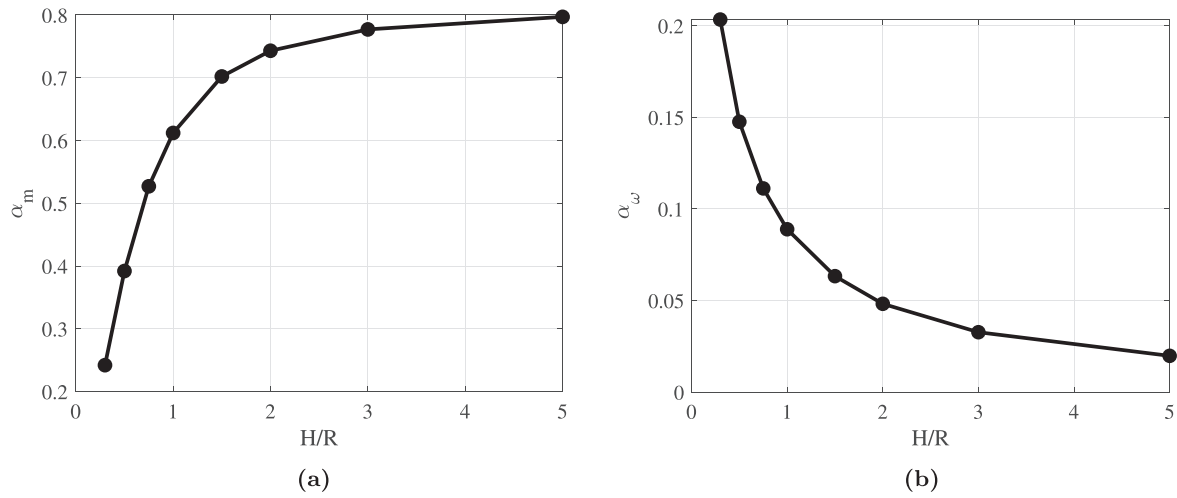


Figure 2. Ratios $\alpha_m = m_b/m_l$ and $\alpha_\omega = \omega_b/\omega_0$ against tank slenderness H/R . The values of α_m and α_ω are tabulated in [5].

Table 1. Main characteristics of the storage tank.

Tank radius	R	4.00	m
Tank height	L	14.00	m
Shell thickness	h	6.00	mm
Liquid height	H	12.00	m
Tank slenderness	H/R	3.00	\
Tank elastic modulus	E_t	210.00	GPa
Tank density	ρ_t	7.85	ton m ⁻³
Liquid density	ρ_l	1.00	ton m ⁻³
Mass of the tank	m_t	18.94	ton
Mass of the liquid	m_l	603.19	ton
Breathing mass	m_b	468.68	ton
Vertical impulsive mass	m_{vi}	134.51	ton
Natural frequency of the breathing mode	ω_b	42.28	rad s ⁻¹
Breathing stiffness	k_b	837.91	kN mm ⁻¹

The hydrodynamic pressure can be calculated following the procedure of EC-8 Part 4 [26]. When the tank is subjected to a vertical ground motion $\ddot{z}_g(t)$, the impulsive fluid pressure reads:

$$p_{vi}(t) = \rho_l H \ddot{z}_g(t), \quad (4)$$

where ρ_l is the liquid density. The contribution due to the radial breathing of the shell is obtained from the following equation:

$$p_{vb}(t) = 0.815[1.078 + 0.274 \cdot \log(H/R)] \rho_l H \ddot{z}_b(t), \quad (5)$$

where $\ddot{z}_b(t)$ is the acceleration of the breathing mass subjected to $\ddot{z}_g(t)$.

The total hydrodynamic base pressure $p_v(t)$ is eventually obtained from equation (1). According to equations (4) and (5), the vertical impulsive mass and the breathing mass give a contribution to the base pressure which is proportional to their acceleration. The acceleration of m_{vi} equals the ground acceleration $\ddot{z}_g(t)$; on the other hand, the breathing mass behaves as a SDoF system which amplifies the base acceleration. Figure 2(a) shows that the percentage of breathing mass increases with the tank slenderness i.e. in a slender tank,

the major part of the contained liquid participates in the breathing mode. Based on these considerations, the breathing mass provides the highest contribution to the base pressure. Therefore, the metafoundation aims at mitigating the breathing mass response.

2.2. Foundation description and modeling

The metafoundation we consider was proposed by Basone *et al* [18] for the isolation of fuel storage tanks against horizontal ground motions and is showed in figure 3. Its horizontal section consists of nine square shaped unit cells of 3 m side, composed by steel hollow columns and 200 mm thick concrete slabs; material properties are shown in table 2. Single-layered and two-layered configurations were examined in depth. In each unit cell, a concrete cube (resonator) is connected to both the upper and lower slab by means of special devices called wire ropes; their indicative layout is sketched in figure 4(a). They consist of a stainless steel cable that is spirally wrapped and blocked by two steel bars as shown in figure 4(b) [27, 28]. Thanks to the mechanical flexibility and spatial configuration of the cable, they can achieve high flexibility in both the horizontal -roll and shear- and vertical -tension-compression- directions. Moreover, because of friction between wires forming the cable, vibrational energy can efficiently be wiped out [29]. So far, in order to characterize both stiffness and strength properties along their principal directions, several experimental and analytical studies were conducted [29–31] One can easily deduce that whilst the horizontal force–displacement relationship is symmetric, their tension-compression behavior exhibits hardening in tension and softening in compression, thus highlighting high asymmetry. Nonetheless, for small relative displacements a linearly elastic symmetric behavior can be assumed, see figure 4(c). Moreover, it is also worth to notice that stiffness values in the three directions are not independent; in particular, roll and shear stiffnesses show a decreasing trend with the increase of the vertical load. Herein, we aim at minimizing the breathing mass response and,

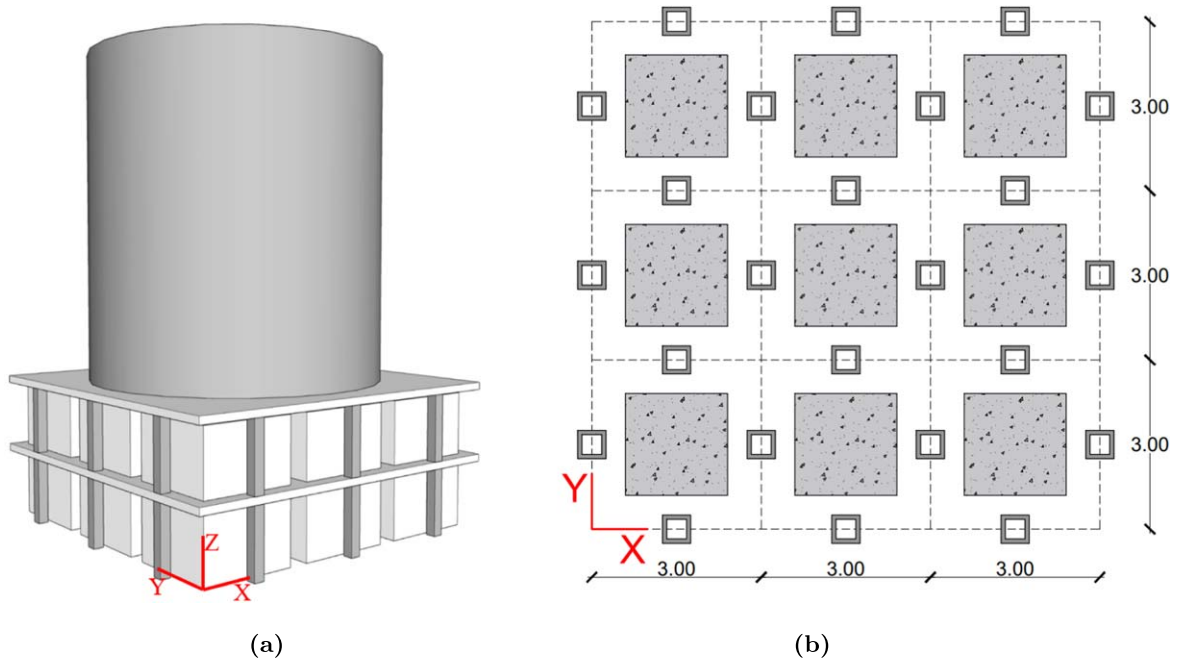


Figure 3. Coupled foundation-tank system proposed in [18]. (a) Isometric view; (b) horizontal section. Dimensions in meters.

Table 2. Mechanical properties of materials.

Material	Density (kg m^{-3})	Elastic modulus (N mm^{-2})	Poisson ratio	Strength (N mm^{-2})
Concrete C40/50	2500	30 000	0.20	40
Steel	7860	200 000	0.28	275
Reinforcement	7850	210 000	0.28	550

therefore, we focus on the optimization of wire ropes' vertical stiffness and damping in the tension-compression direction.

In accordance with base isolation theory and the results of [18], a low stiffness connection between the superstructure and the soil reduces the seismic response. In the analyzed case, this requires the reduction of the foundation outer frame vertical stiffness, which is controlled by the axial stiffness of the columns. A possible way to achieve this goal is to take advantage of the slabs flexural stiffness, which is lower than the columns axial stiffness. To this end, columns at the first level are located at the vertex of the square projection of every unit cell, while those at the second level are staggered with respect to the previous ones. Table 3 compares the aligned-columns and the staggered-columns cases. We study five possible configurations, distinguished by the number of layers ('L1' = single-layered, 'L2' = two-layered), the total foundation frame height ('H3' = 3 m height, 'H4' = 4 m height) and the columns arrangement ('a' = aligned, 's' = staggered): L1H3, L2H4a, L2H3a, L2H4s, L2H3s. Their properties are summarized in table 4.

The dynamic modeling of the foundation is carried out by condensing both masses and stiffnesses of resonators, slabs and columns at each layer to one stack of unit cells. Staggered solutions vertical stiffness depends on the in-series combination of columns axial stiffness and slabs flexural stiffness: it is determined by applying Force Method to the FE model described in section 2.5. The main properties of the condensed model are

summarized in table 5, where: m_{11} and m_{12} are the condensed masses (columns and slab) at the first and second level, respectively; k_1 is the condensed stiffness of the columns at the first level; k_{1s} is the condensed stiffness of the columns (or in-series column slab elements, for the staggered configuration) at the second level; m_2 and k_2 are the condensed masses and stiffnesses of the resonators. It can be observed that the staggered stiffnesses are about one order of magnitude smaller than the aligned ones.

2.3. Coupled systems and equations of motion (EOM)

The condensed dynamic models of coupled foundation-tank systems are shown in figure 5. The vertical impulsive mass and the mass of the tank are rigidly attached to the foundation superior slab; resonators are connected to slabs through springs k_2 and dashpots $c_2 = 2\xi_2\sqrt{k_2m_2}$. The system of EOM for the coupled structure subjected to a vertical ground motion $\ddot{z}_g(t)$ can be written as:

$$\mathbf{M}\ddot{\mathbf{w}}(t) + \mathbf{C}\dot{\mathbf{w}}(t) + \mathbf{K}\mathbf{w}(t) = -\mathbf{M}\boldsymbol{\tau}\ddot{z}_g(t), \quad (6)$$

where \mathbf{M} , \mathbf{C} and \mathbf{K} denote the mass, damping and stiffness matrices; $\ddot{\mathbf{w}}(t)$, $\dot{\mathbf{w}}(t)$ and $\mathbf{w}(t)$ represent the relative acceleration, velocity and displacement vectors with respect to the ground motion $\ddot{z}_g(t)$; $\boldsymbol{\tau}$ is the dragging vector, which equals the unitary vector because the inertial acceleration is applied to each mass of

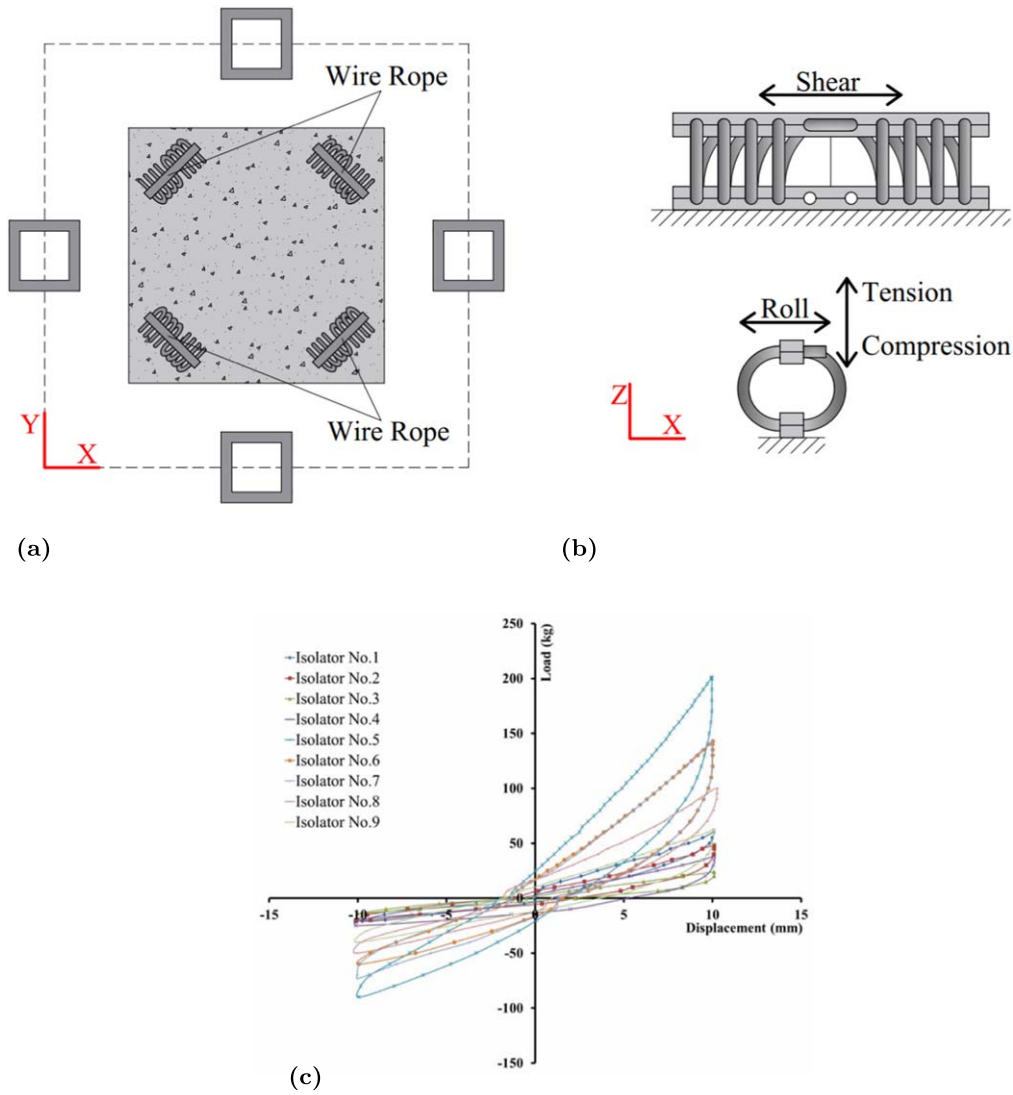


Figure 4. Wire ropes used to link resonators: (a) arrangement in a unit cell; (b) geometrical and kinematic details; (c) hysteretic behavior under tension-compression loading (after [29]).

the model. For the single-layered configuration:

$$\begin{aligned}
 \mathbf{w}(t) &= [w_1(t), w_b(t), w_2(t)]^T, \\
 \mathbf{M} &= \begin{bmatrix} m_1 + m_t + m_{vi} & 0 & 0 \\ 0 & m_b & 0 \\ 0 & 0 & m_2 \end{bmatrix}; \\
 \mathbf{K} &= \begin{bmatrix} k_1 + k_2 + k_b & -k_b & -k_2 \\ -k_b & k_b & 0 \\ -k_2 & 0 & k_2 \end{bmatrix}.
 \end{aligned}
 \tag{8}$$

For the two-layered systems:

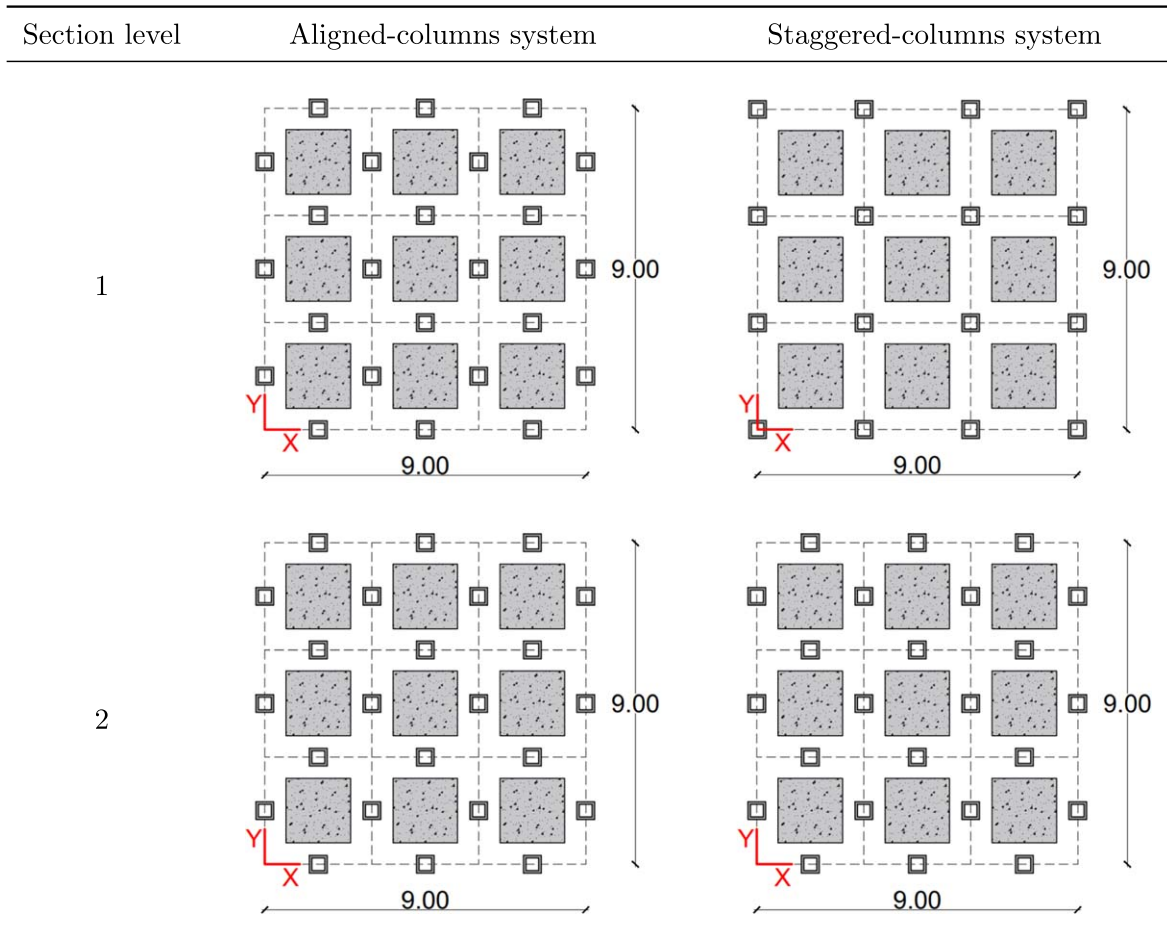
$$\begin{aligned}
 \mathbf{w}(t) &= [w_{11}(t), w_{12}, w_b(t), w_{21}(t), w_{22}(t)]^T, \\
 \mathbf{M} &= \begin{bmatrix} m_{11} & 0 & 0 & 0 & 0 \\ 0 & m_{12} + m_t + m_{vi} & 0 & 0 & 0 \\ 0 & 0 & m_b & 0 & 0 \\ 0 & 0 & 0 & m_2 & 0 \\ 0 & 0 & 0 & 0 & m_2 \end{bmatrix},
 \end{aligned}
 \tag{10}$$

$$\mathbf{K} = \begin{bmatrix} k_1 + k_{1s} + 2k_2 & -k_{1s} & 0 & -k_2 & -k_2 \\ -k_{1s} & k_{1s} + k_b + k_2 & -k_b & 0 & -k_2 \\ 0 & -k_b & k_b & 0 & 0 \\ -k_2 & 0 & 0 & 2k_2 & 0 \\ -k_2 & -k_2 & 0 & 0 & 2k_2 \end{bmatrix}.
 \tag{11}$$

In the configuration with aligned columns, $k_{1s} = k_1$. Regarding the matrix \mathbf{C} , we adopted a non-classical damping model in which damping and stiffness matrices have the same shape. This allows for direct assignation of damping to the resonators and simplifies the design.

2.4. Site-specific seismic hazard and accelerograms selection

The tank investigated in this research is located in the refinery of Priolo Gargallo, Italy, where the soil is classified as Type B according to the Italian standards [19]. In order to evaluate the seismic activity at the construction site, we consider: (i) a set of natural accelerograms with 10% probability of exceedance

Table 3. Comparison between aligned-columns and staggered-columns system.**Table 4.** Geometrical characteristics of the studied metafoundations.

Foundation	L1H3	L2H4a	L2H3a	L2H4s	L2H3s
Layers	1	2	2	2	2
Height of one layer (m)	3	2	1.5	2	1.5
Slab thickness (mm)	200	200	200	230	230
Column side (mm)	250	230	200	230	200
Column thickness (mm)	30	30	30	40	35
Columns at layer 1	24	24	24	16	16
Columns at layer 2	0	24	24	24	24

Table 5. Properties of the metafoundations dynamic models.

Foundation	L1H3	L2H4a	L2H3a	L2H4s	L2H3s
m_{11} (ton)	57.48	50.91	47.29	54.67	51.86
m_{12} (ton)	\	50.91	47.29	58.72	54.50
m_2 (ton)	267.91	178.61	133.95	178.61	133.95
k_1 (kN mm ⁻¹)	144 000	66 240	57 600	51 520	44 800
k_{1s} (kN mm ⁻¹)	\	66 240	57 600	5389	4578

in 50 years, i.e. the operating basis earthquakes OBE (Acc1-Acc7); (ii) a set of natural accelerograms with 5% probability of exceedance in 50 years, i.e. the safe shutdown earthquakes SSE (Acc.8-Acc.13). The two sets of signals are listed in

table 6. They were selected so that their mean spectrum fits in a leastsquare sense the horizontal uniform hazard spectrum (UHS) of the site. In section 4.2.2, they are used to obtain Soil Model #2; moreover, in section 5, they are implemented to evaluate the response of the superstructure in time domain.

The UHS is obtained as the envelope of spectral amplitudes of accelerograms at all periods that are exceeded with a certain probability for a certain number of years [32]. More precisely, 2% probability in 50 years for the SSE. Therefore, the UHS is often overly conservative because it combines the hazard from different sources and does not reflect a realistic spectrum that can be expected to occur during a single earthquake at a certain period. As a result, when seismic records derived from a UHS

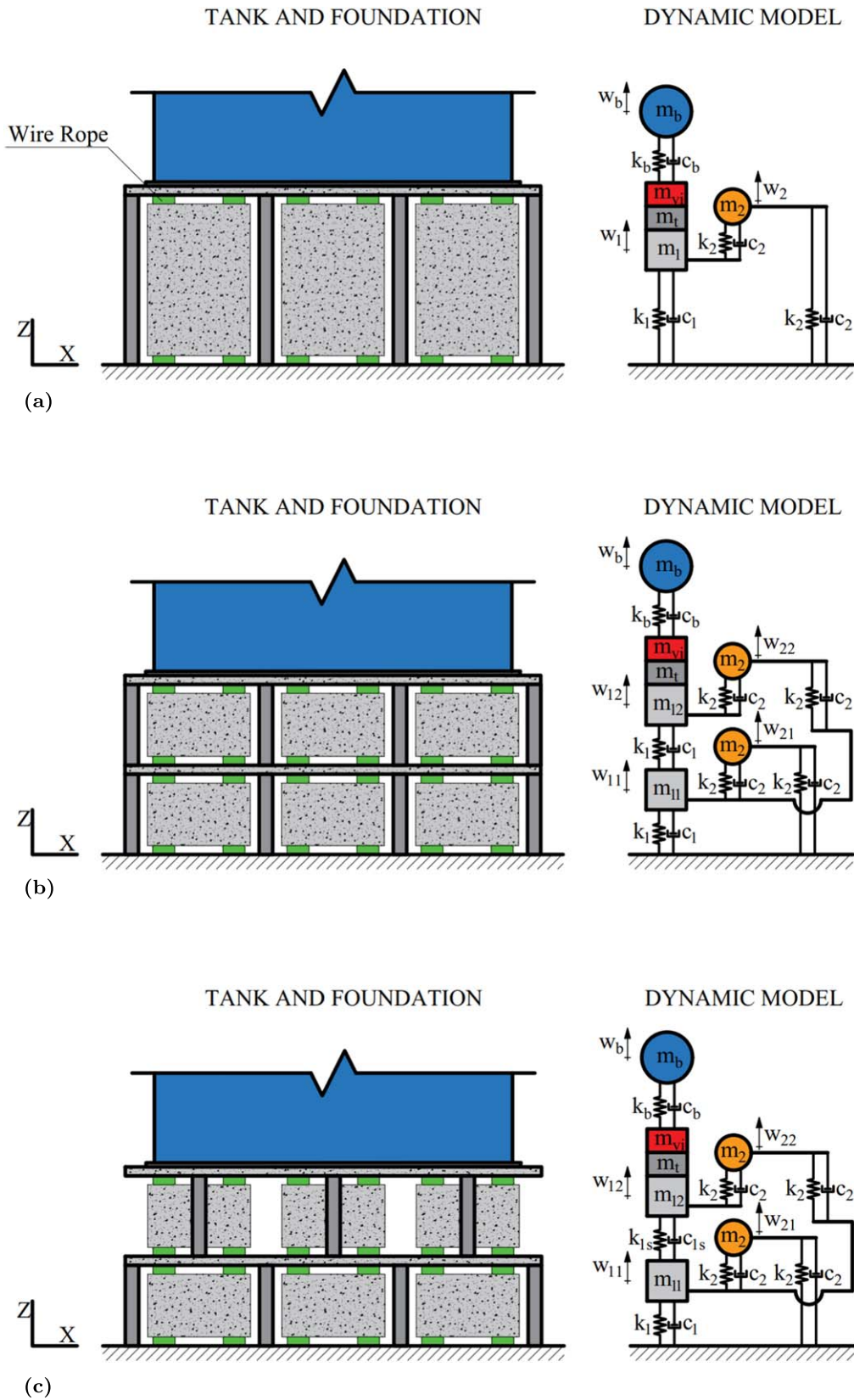


Figure 5. Coupled foundation-tank systems. (a) L1; (b) L2a; (c) L2s.

are considered in the optimization process of section 4 and for time history analysis in section 5, it is not deemed necessary to use a conditional mean spectrum that matches the UHS level

only at the fundamental period of a system. Both the vertical response spectra of the selected accelerograms and the relevant UHS of Priolo Gargallo are shown in figure 6.

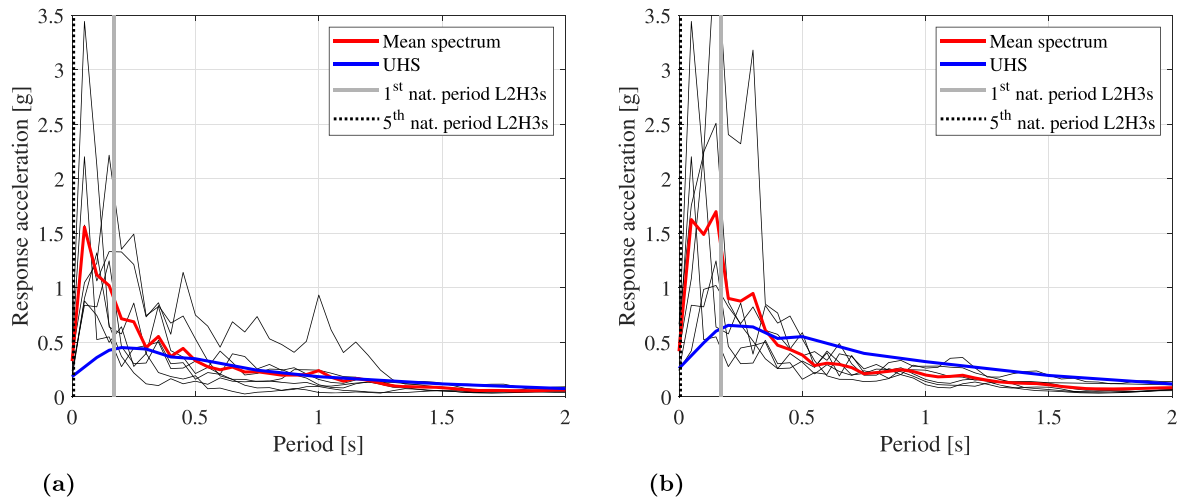


Figure 6. Response spectra and mean spectrum of the selected accelerograms and vertical UHS of Priolo Gargallo: (a) OBE signals; (b) SSE signals.

Table 6. List of natural accelerograms for OBE and SSE events.

Acronym	Event	Country	Magnitude M_w	PGA (m s^{-2})	Type
Acc1	South Iceland Aftershock	Island	6.4	3.71	OBE
Acc2	South Iceland	Island	6.5	1.78	OBE
Acc3	Ano Liosia	Greece	6.0	1.93	OBE
Acc4	L'Aquila Mainshock	Italy	6.3	4.35	OBE
Acc5	L'Aquila Mainshock	Italy	6.3	2.35	OBE
Acc6	L'Aquila Mainshock	Italy	6.3	3.55	OBE
Acc7	L'Aquila Mainshock	Italy	6.3	4.87	OBE
Acc8	Northridge-01	USA	6.7	2.43	SSE
Acc9	South Iceland	Island	6.5	6.54	SSE
Acc10	Landers	USA	7.3	4.12	SSE
Acc11	L'Aquila Mainshock	Italy	6.3	4.35	SSE
Acc12	L'Aquila Mainshock	Italy	6.3	2.35	SSE
Acc13	L'Aquila Mainshock	Italy	6.3	4.87	SSE

2.5. Seismic design of the metafoundation

As stated in section 2.2, to reduce vertical stiffness and improve seismic isolation performance, we propose a staggered-columns arrangement. Because of the high dead load exerted by the tank, a complex stress distribution is expected in the two slabs, especially at the first level, where the second level columns act as point loads. The slabs thickness was increased to 230 mm, as shown in table 4. In order to evaluate stress distributions, we set a FE model with the software ETABS [33]. Columns and slabs were modeled by means of frame elements and thin-shell elements, respectively. In accordance with the indications provided in [34, 26], in order to take into account concrete cracking under seismic loading, the elastic modulus of concrete shells was reduced by 50%. The tank was modeled as a shell load of 122 kN m^{-2} acting within the perimeter of its base slab. Moreover, every resonator of weight W_R was modeled by means of four concentrated

loads with magnitude $W_R/4$ acting in the vertical direction. The response spectrum method was used to model the seismic action in the vertical direction, considering a return period $T_R = 2475\text{y}$ and the parameters prescribed by NTC 2018 [19]. As a result, columns were designed to remain elastic.

Figures 7(a), (b) depict the m_{yy} resultant moment distribution in the two slabs. The required bending reinforcement in the x direction was calculated considering 1.5 m width strips and is shown in figures 7(c), (d). Because of the symmetry of the problem, the same amount of reinforcement was required in the y direction. With reference to figure 7(e) and table 7, patterned circles and squares represent the required punching shear reinforcement and drop panels, which were designed according to EC-2 [34]. Details #1, #2 and #3 refer to the geometric properties shown in figure 8. More precisely, to realize the connection between columns and concrete slabs, a plate with shear studs was welded at the columns head. The enlarged plate depicted in figure 8(a) was

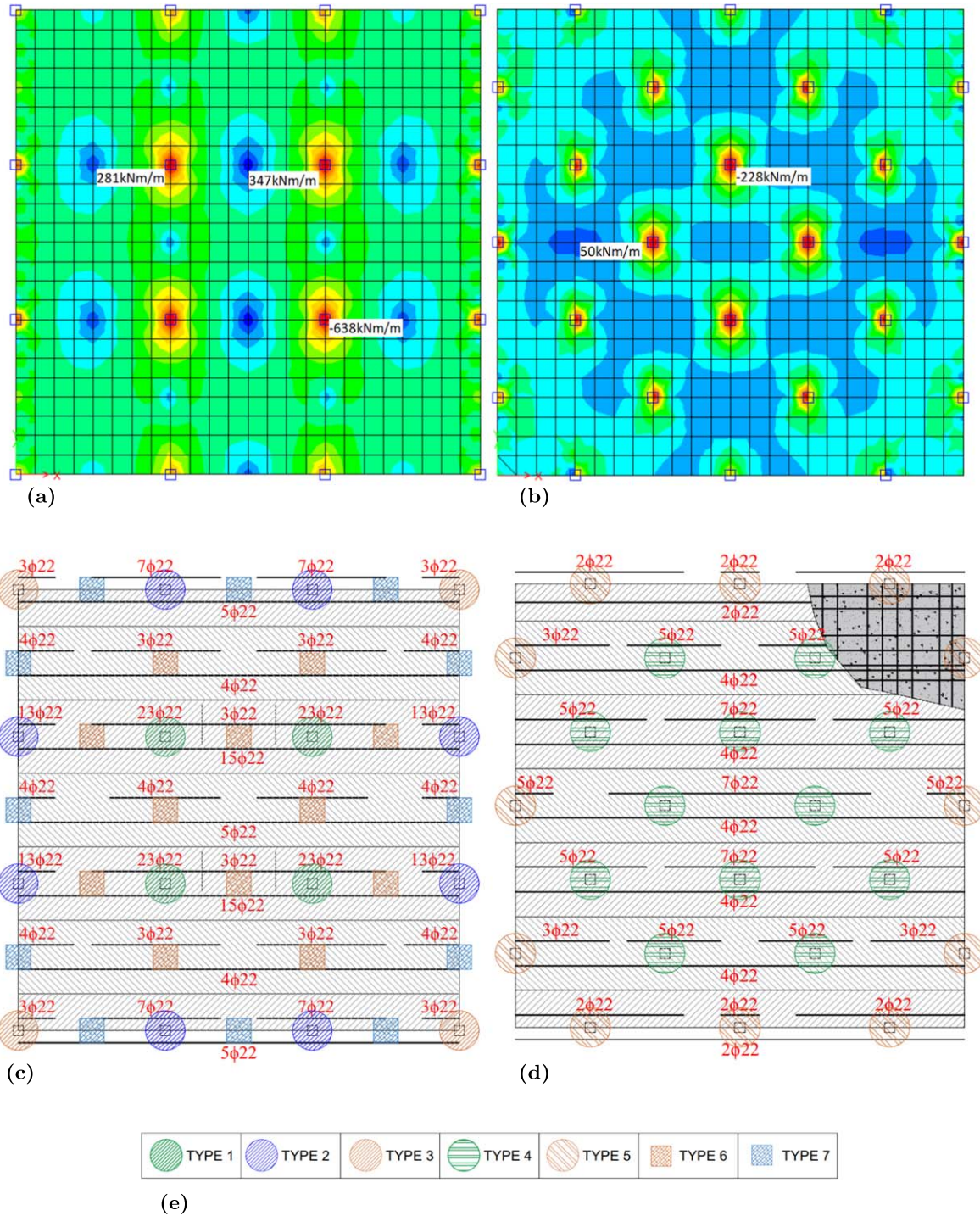


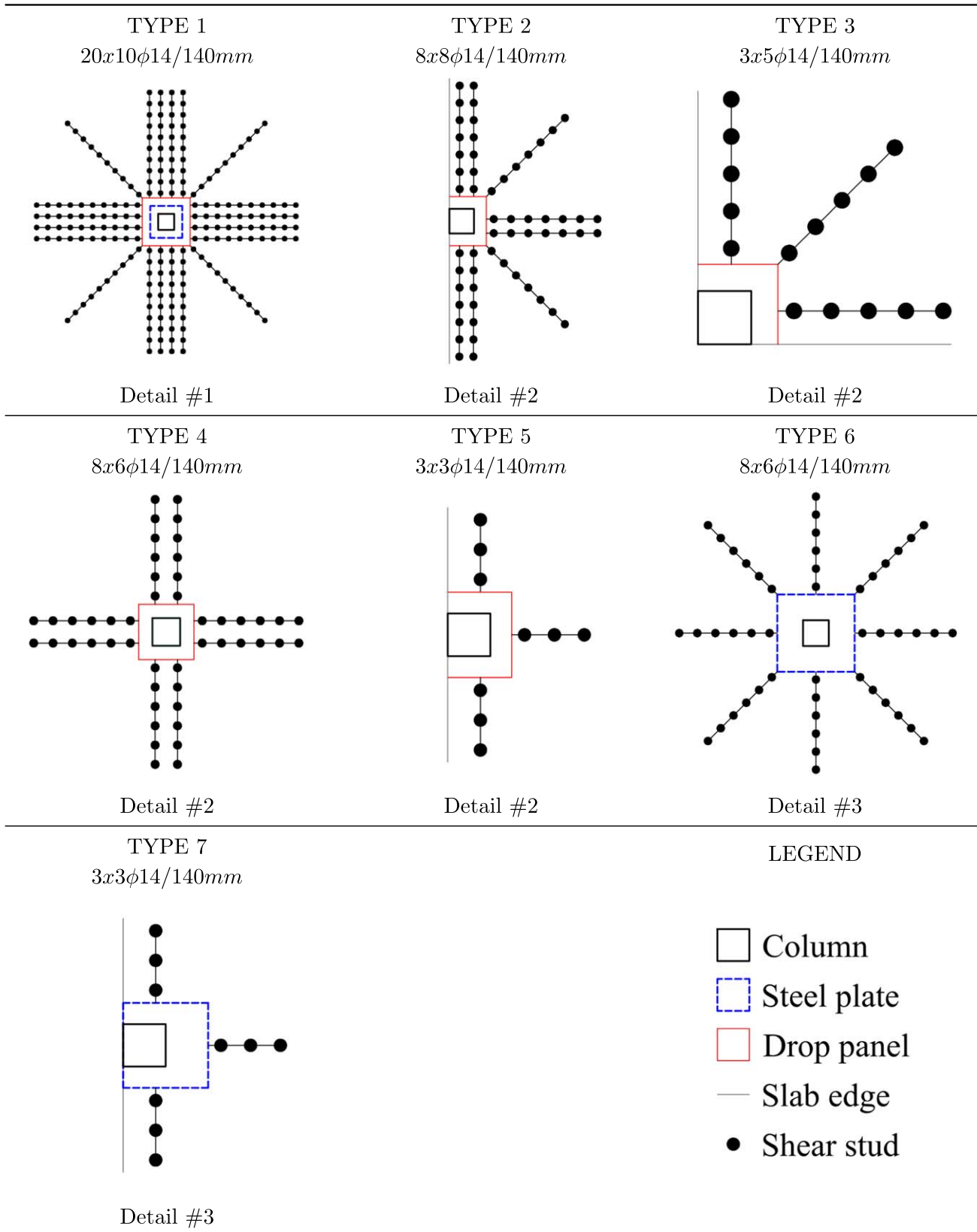
Figure 7. Slabs design. Resultant bending moment m_{yy} on first (a) and second (b) level slab; bending reinforcement in first (c) and second (d) level slab; (e) legend for punching shear reinforcement, which refers to table 7.

used in locations where the punching load was particularly high, while figure 8(b) shows the detail for other cases. Figure 8(c) shows the connection between the second level staggered columns and the first level slab; there, a plate was welded to the column base and connected to the slab by means of studs. Finally, stiffeners allowed a better distribution of punching load so as to avoid drop panels.

3. Metamaterials and periodic lattice concept

Locally resonant metafoundations are inspired by metamaterials, which act as band pass filters on propagating signals by suppressing elastic wave propagation in band gaps. Band gaps can be determined by means of dispersion analysis using Bloch's Theorem.

Table 7. Punching shear reinforcement. Detail 1, 2 and 3 are depicted in figure 8.



Consider the infinite periodic 1D lattice shown in figure 9(a). A unit cell consists of an external mass m_1 and an internal resonator with mass m_2 and stiffness k_2 . The external

masses are connected by means of springs k_1 and unit cells are uniformly placed with a periodic distance constant L . The EOM of the j th unit cell in vertical direction can be written as:

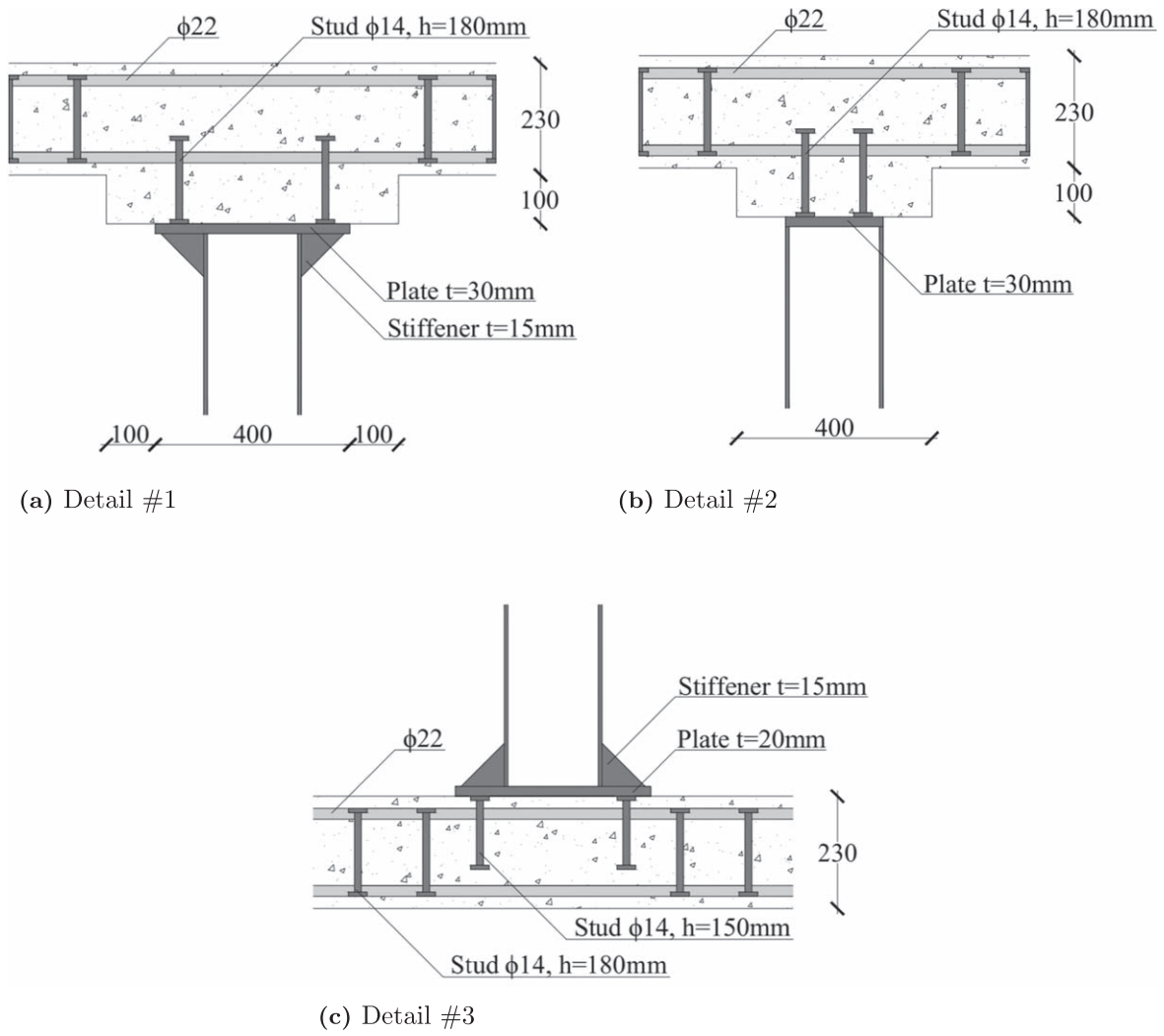


Figure 8. Details of drop panels and slab-to-column connections.

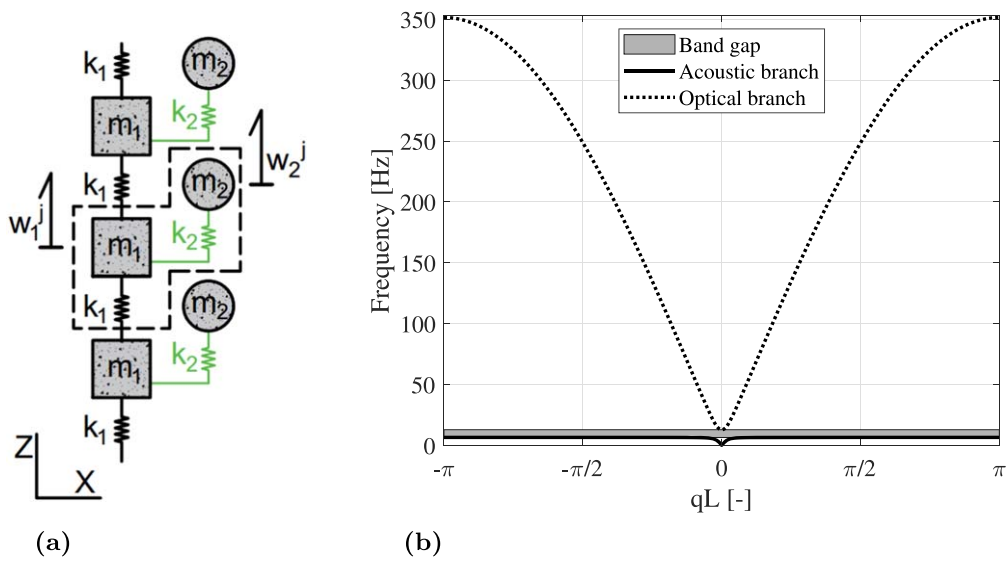


Figure 9. Infinite periodic 1D lattice. (a) Mass-spring model; (b) dispersion relation.

$$\begin{cases} m_1 \ddot{w}_1^j + k_1(w_1^j - w_1^{j-1}) + k_1(w_1^j - w_1^{j+1}) + k_2(w_1^j - w_2^j) = 0 \\ m_2 \ddot{w}_2^j + k_2(w_2^j - w_1^j) = 0 \end{cases} \quad (12)$$

According to Bloch's theorem [35], the harmonic wave solution for the $(j + n)$ th unit cell reads:

$$u_\gamma^{(j+n)} = B_\gamma \cdot e^{i(qx+nqL-\omega t)}, \quad (13)$$

where B_γ is the complex wave amplitude, i the imaginary unit, q the wave number, ω the circular frequency and $\gamma = 1, 2$. By substituting equation (13) into equation (12) and applying Euler's formula, the eigenproblem $(-\omega^2 \mathbf{M} + \mathbf{K})\mathbf{B} = \mathbf{0}$ is obtained. Its characteristic polynomial results:

$$\begin{aligned} \omega^4 m_1 m_2 - \omega^2 [(m_1 + m_2)k_2 + 2m_2 k_1 (1 - \cos qL)] \\ + 2k_1 k_2 (1 - \cos qL) = 0. \end{aligned} \quad (14)$$

The positive solutions of equation (14) yield the dispersion relation, which relates the frequency of wave propagation across the lattice to the wave number q . As an example, by substituting condensed parameters of the configuration L2H3a into equation (14), the dispersion relation of the corresponding infinite lattice can be obtained, as shown in figure 9(b). A band gap is observed within 6.56 and 12.85 Hz. The lower and the upper bounds of the band gap are defined lower bound frequency (LBF) and upper bound frequency (UBF), respectively.

4. Metafoundation optimization in frequency domain

4.1. General considerations

In this section, we develop an optimization procedure aiming to minimize the variance of the breathing mass absolute acceleration response. With reference to section 2.2, the invariant parameters of the model are the masses m_{11} , m_{12} and m_2 , the stiffnesses k_1 and k_{1s} and the damping coefficient c_1 ; we optimize the natural frequency $\omega_2 = \sqrt{k_2/m_2}$ and the damping factor ξ_2 of the resonators. In order to compute the breathing mass response's variance, we need a power spectral density (PSD) function $S_g(\omega)$, such as to simulate the filtering properties of a soil layer. Among the filters available, section 4.2.1 suggests Soil Model #1 which relies on the Kanai-Tajimi filter; its parameters are selected to broadly represent soil properties in the presence of the vertical component of seismic acceleration. Therefore, the influence of soil properties on the performance of metafoundations can be taken into account. Moreover, we propose Soil Model #2 in section 4.2.2; it assumes that soil properties depend only on the contribution to the vertical acceleration provided by P-waves. The aforementioned models are adopted for the definition of PSDs functions for OBE and SSE earthquakes at the location of Priolo Gargallo. Therefore, given the use of the vertical component of site-specific accelerograms, metafoundations optimized by means of Soil Model #2 are expected to be more accurate. The Performance Index PI for the optimization is defined in section 4.3 and, finally, optimal

Table 8. Parameters of the Kanai-Tajimi filter.

Soil type	S_0	ω_g (rad s ⁻¹)	ξ_g
Dense	0.013	38.80	0.46
Medium	0.018	29.10	0.46
Loose	0.020	26.20	0.46

parameters of the metafoundations are presented in section 4.4.

4.2. Soil models

4.2.1. Soil model #1: Kanai-Tajimi. Kanai and Tajimi [36] proposed an analytical formulation able to simulate a sitespecific PSD as stationary Gaussianfiltered white noise random process with zero mean and spectral intensity S_0 . In detail, to model the properties of the soil layer, they suggested the following filter formulation:

$$H_{KT}(\omega) = \frac{1 + 2 \cdot i \xi_g \frac{\omega}{\omega_g}}{\left(1 - \frac{\omega^2}{\omega_g^2}\right) + 2 \cdot i \xi_g \frac{\omega}{\omega_g}}, \quad (15)$$

where ω_g , ξ_g represent the natural frequency and damping ratio of the soil layer, respectively. Multiplying the filter with a white noise process S_0 , which represents excitation at the bedrock, the PSD model at the surface reads:

$$S_{g,KT}(\omega) = S_0 \cdot |H_{KT}(\omega)|^2. \quad (16)$$

In order to represent the PSD of vertical ground motions, we chose the parameters of table 8 from [37].

4.2.2. Soil model #2: 1D pressure waves. In order to take into account the geotechnical properties of soil and rock and the seismic hazard at the construction site, the PSD of a natural accelerogram vertical component $S_{g,real,i}(\omega)$ is multiplied by the transfer function of the soil layer. This approach is valid under the hypothesis that the ground motion vertical component is generated only by pressure waves, which propagate from the bedrock to the surface of a horizontal soil stratum. This assumption is justified from the fact that a seismogram contains three components and, among them, one can find a major contribution of P-waves to the vertical component. In the other two components, one can observe major contributions from both S-waves and surface waves. For the case of a uniform damped soil layer of thickness L which lays on an elastic bedrock, the transfer function can be expressed as [37]:

$$H_P(\omega) = \frac{1}{\cos\left(\frac{\omega L}{c_2}\right) + i \frac{\rho_2 c_2}{\rho_1 c_1} \sin\left(\frac{\omega L}{c_2}\right)}, \quad (17)$$

where: c_1 and c_2 are the propagation speeds of the P waves in the bedrock and in the soil layer, respectively; ρ_1 and ρ_2 are the volume densities of the corresponding materials. Based on the analysis of [38, 39], we considered the following parameters:

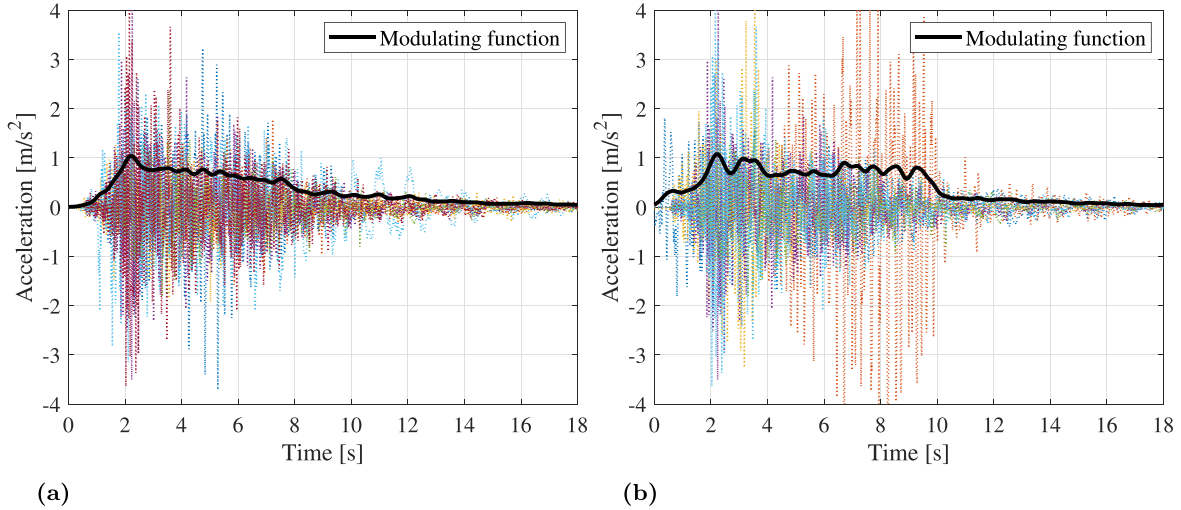


Figure 10. Accelerograms sets and estimate of the time modulating function $\tilde{\phi}(t)$. (a) OBE signals; (b) SSE signals.

$c_1 = 1559 \text{ m s}^{-1}$, $\rho_1 = 2300 \text{ kg m}^{-3}$, $c_2 = 814 \text{ m s}^{-1}$, $\rho_2 = 2000 \text{ kg m}^{-3}$, $L = 30 \text{ m}$.

The variance of the response is calculated in the assumption of stationary process. Hence, the previously mentioned $S_{g,real,i}(\omega)$, that is to be multiplied by the filter $H_P(\omega)$, should be the PSD of a stationary real accelerogram. The non-stationary PSD function can be written as:

$$S_{non-st}(\omega, t) = \phi^2(t) \cdot S_{st}(\omega), \quad (18)$$

where $\phi(t)$ is a time modulating function and $S_{st}(\omega)$ is the stationary PSD. Considering a set of N natural accelerograms $\ddot{z}_{g,i}(t)$, $i = 1, 2, \dots, N$, an estimate $\tilde{\phi}(t)$ of $\phi(t)$ is:

$$\tilde{\phi}(t) = \frac{\tilde{\sigma}(t)}{\max\{\tilde{\sigma}(t) | t \in [0, T]\}}. \quad (19)$$

In this equation, $\tilde{\sigma}(t)$ represents the estimate of the standard deviation of the recorded signals, while T is the time duration of the process. A set of pseudostationary signals can then be evaluated by means of the following formulation:

$$\ddot{z}_{g,st,i}(t) = \frac{\ddot{z}_{g,i}(t)}{\tilde{\phi}(t)}. \quad (20)$$

Eventually, each pseudostationary PSD function is calculated as the Fourier transform of the autocorrelation of each signal $\ddot{z}_{g,st,i}(t)$, as follows [18]:

$$S_{g,real,i}(\omega_p) = \frac{1}{M^2 \Delta \omega_p} \left| \sum_{k=1}^M [\ddot{z}_{g,st,i}(t_k) \cdot \exp\{-i\omega_p t_k\}] \right|^2, \quad (21)$$

where ω_p is the sampled frequency with frequency increment $\Delta \omega$ and M is the total amount of time steps t_k of the signal.

As discussed in section 2.4, we considered: (i) a set of $N_{OBE} = 7$ accelerograms whose mean response spectrum fits the OBE spectrum of Priolo Gargallo; (ii) a set of $N_{SSE} = 6$ accelerograms whose mean response spectrum fits the SSE spectrum of Priolo Gargallo. Figure 10 depicts the resulting time modulating functions $\tilde{\phi}(t)$ and the two accelerograms sets. From them, we obtained the pseudostationary PSD

functions $S_{g,real,OBE,i}(\omega)$ and $S_{g,real,SSE,i}(\omega)$. They can be averaged to calculate the average pseudostationary PSDs:

$$\bar{S}_{g,real,OBE} = \text{mean}\{S_{g,real,OBE,i}\} | i, \quad i = 1, 2, \dots, N_{OBE} \quad (22)$$

$$\bar{S}_{g,real,SSE} = \text{mean}\{S_{g,real,SSE,i}\} | i, \quad i = 1, 2, \dots, N_{SSE}. \quad (23)$$

Multiplying the average pseudostationary PSDs by the filter $H_P(\omega)$, the PSD models for 1D P waves read:

$$S_{g,P,OBE} = |H_P(\omega)|^2 \cdot \bar{S}_{g,real,OBE}, \quad (24)$$

$$S_{g,P,SSE} = |H_P(\omega)|^2 \cdot \bar{S}_{g,real,SSE}. \quad (25)$$

Figure 11(a) compares the soil filters $|H_P(\omega)|^2$ and $|H_{KT}(\omega)|^2$; the resulting PSD models for the optimization (equations (16), (24) and (25)) are shown in figure 11(b).

4.3. Optimization procedure

By assuming an excitation accelerogram to be a limited duration segment of a stationary random function with PSD $S_g(\omega)$, the PSD of the structure response measured at the i th DoF results [40]:

$$S_i(\omega) = S_g(\omega) |H_i(\omega)|^2, \quad (26)$$

where $H_i(\omega)$ is the transfer function of the considered DoF. As stated above, the breathing mass gives the highest contribution to the base pressure of a slender tank. Hence, we develop the optimization procedure with reference to its absolute vertical acceleration, whose transfer function is $\ddot{Z}_b(\omega)$. By assuming a zero-mean process, the integral over frequency of the PSD represents the average total power, or variance of the absolute acceleration response:

$$\sigma_{\ddot{Z}_b}^2 = \int_0^\infty S_b(\omega) d\omega = \int_0^\infty S_g(\omega) |\ddot{Z}_b(\omega)|^2 d\omega. \quad (27)$$

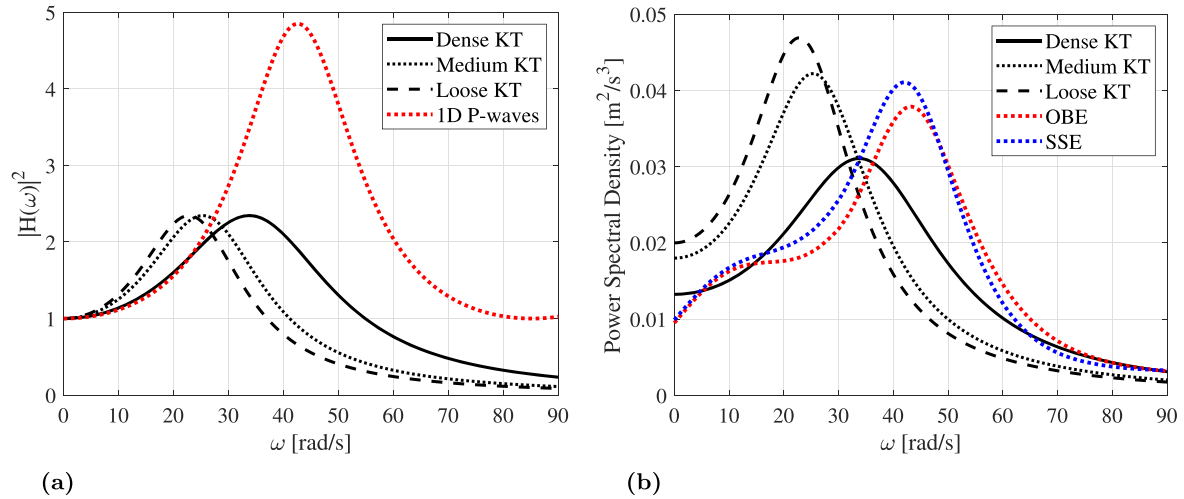


Figure 11. (a) Soil layer filters $|H_{KT}(\omega)|^2$ and $|H_P(\omega)|^2$; (b) PSD models.

When the system is subjected to an harmonic excitation $\ddot{z}_g(t) = e^{i\omega t}$, the steady state structural response results $\mathbf{w}(t) = \mathbf{W}(\omega)e^{i\omega t}$, where $\mathbf{W}(\omega)$ is the transfer function of the relative displacement. Substituting in equation (6) and solving with respect to $\mathbf{W}(\omega)$, the following formulation is obtained:

$$\mathbf{W}(\omega) = (-\omega^2\mathbf{M} + i \cdot \omega\mathbf{C} + \mathbf{K})^{-1}(-\mathbf{M} \boldsymbol{\tau}). \quad (28)$$

Deriving the relative displacement $\mathbf{w}(t)$ with respect to time, the relative acceleration results $\ddot{\mathbf{w}}(t) = -\omega^2\mathbf{W}(\omega)e^{i\omega t} = \ddot{\mathbf{W}}(\omega)e^{i\omega t}$, in which $\ddot{\mathbf{W}}(\omega)$ defines the relative acceleration transfer function. The absolute acceleration transfer function is obtained by summation of relative and ground accelerations:

$$\ddot{\mathbf{Z}}(\omega) = \boldsymbol{\tau} - \omega^2\mathbf{W}(\omega). \quad (29)$$

Eventually, we defined PI as:

$$\text{PI}(\omega_2, \xi_2) = \frac{\sigma_{Z_{b,c}}^2(\omega_2, \xi_2)}{\sigma_{Z_{b,u}}^2}, \quad (30)$$

where: $\sigma_{Z_{b,c}}^2$ is the variance of the absolute vertical acceleration response of the breathing mass controlled by one of the metafoundations described in section 2.2; $\sigma_{Z_{b,u}}^2$ is the variance of the absolute vertical acceleration response of the breathing mass when the tank lays on the free field (fixed base tank). The optimal parameters are those which minimize PI, that is:

$$(\omega_2)_{opt}, (\xi_2)_{opt} = \min[\text{PI}(\omega_2, \xi_2)]. \quad (31)$$

4.4. Optimization results

PI is numerically computed as a function of the tuning frequency ω_2 and the damping ratio ξ_2 of resonators. Figure 12 depicts the PI surface for the foundation L2H3s on dense soil and the corresponding contour lines. The optimal parameters for all analyzed systems and minimum values of PI are listed in table 9. In particular, it shows that the PI can be lower than 1 and, therefore, it is possible to design a vertically-efficient

metafoundation; hence, these foundations are able to mitigate the vertical response of superstructures. The natural periods of the optimized coupled foundation-tank systems are collected in table 10. Since L1H3 is a 3DoF system, it is endowed with only three periods; conversely, all remaining metafoundations are characterized by five natural periods. In order to confirm the effectiveness of the accelerograms selected in section 2.4, for the considered coupled foundation-tank systems, both the 1st and the 5th period of L2H3s are plotted in figure 6. In this respect, a careful reader can note that the mean response spectrum is conservatively higher than the vertical UHS in the relevant range of periods. The same consideration applies for the remaining coupled foundation-tank systems.

Figure 12(b) shows that contours are elongated in the ξ_2 axis direction; this points out that the parameter ξ_2 is less influential than the tuning frequency of resonators. Softer systems require higher optimal damping. Moreover, these results show that optimal frequencies of resonators are directly coupled to the foundation frequency.

The optimal parameters of a certain configuration slightly depend on the soil type because of the high stiffness of the foundation outer frame in the vertical direction, which allows for a limited decoupling between the breathing frequency of the tank and the main eigenfrequency of the ground. Better performances are achieved on stiffer soils, where the decoupling is maximum. The nomenclature ‘Dense’, ‘Medium’, ‘Loose’, ‘OBE’ and ‘SSE’ of table 9 refer to the PSD models defined in equations (16), (24) and (25), respectively. For each of them, the minimum value of PI exhibits a decreasing trend from the single-layered design to the staggered-columns one. This reduction shows that, for a given soil type, the outer frame stiffness reduction improves the vertical waves attenuation capacity of the metafoundation. In fact, a soft foundation on stiff soil accomplishes the maximum decoupling between soil frequency content and breathing frequency of a tank. The lowest PI values are achieved with the parameters calculated by means of 1D P-waves PSD model, see

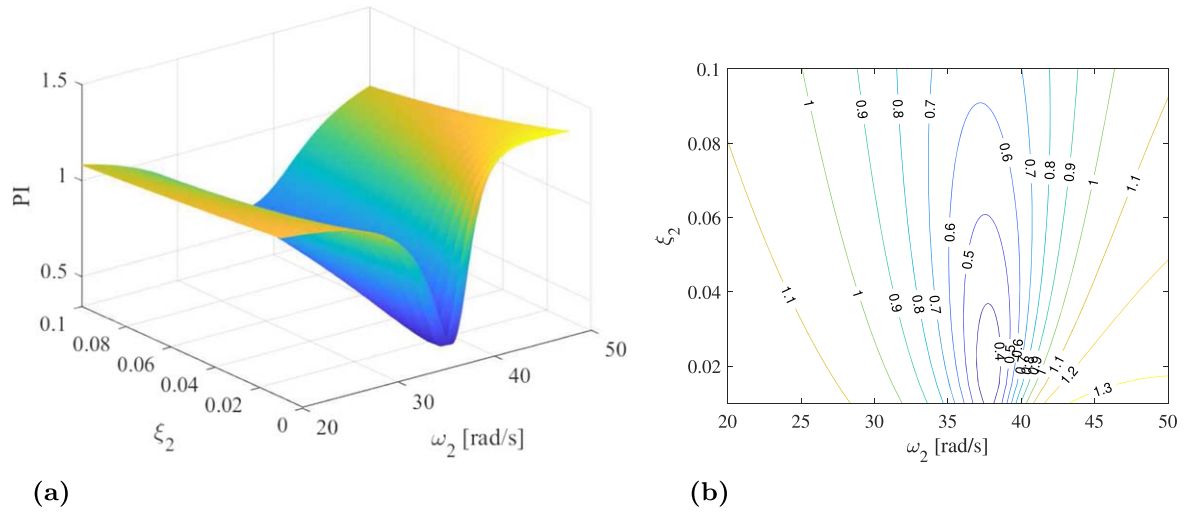


Figure 12. Performance index PI for the foundation L2H3s on dense soil. (a) Optimization surface against resonator parameters; (b) contour lines.

Table 9. Optimal parameters and corresponding minimum values of the performance index.

Type of soil	Optimal parameters	Single-layered				
		L1H3	L2H4a	L2H3a	L2H4s	L2H3s
Dense	$(\omega_2)_{opt}$, rad s ⁻¹	41.44	41.28	41.24	38.28	37.82
	$(\xi_2)_{opt}$	0.01	0.01	0.01	0.02	0.02
	min{PI}	0.968	0.718	0.739	0.337	0.344
Medium	$(\omega_2)_{opt}$, rad s ⁻¹	41.44	41.27	41.24	38.25	37.79
	$(\xi_2)_{opt}$	0.01	0.01	0.01	0.02	0.02
	min{PI}	0.972	0.736	0.759	0.398	0.414
Loose	$(\omega_2)_{opt}$, rad s ⁻¹	41.44	41.27	41.24	38.24	37.79
	$(\xi_2)_{opt}$	0.01	0.01	0.01	0.02	0.02
	min{PI}	0.972	0.739	0.761	0.408	0.426
OBE	$(\omega_2)_{opt}$, rad s ⁻¹	41.45	41.28	41.25	38.34	37.87
	$(\xi_2)_{opt}$	0.01	0.01	0.01	0.02	0.02
	min{PI}	0.961	0.693	0.711	0.268	0.265
SSE	$(\omega_2)_{opt}$, rad s ⁻¹	41.44	41.28	41.25	38.33	37.86
	$(\xi_2)_{opt}$	0.01	0.01	0.01	0.02	0.02
	min{PI}	0.962	0.698	0.717	0.278	0.276

Table 10. Natural periods of the optimized coupled foundation-tank systems.

Foundation period	L1H3 (s)	L2H4a (s)	L2H3a (s)	L2H4s (s)	L2H3s (s)
1st	0.152	0.153	0.153	0.168	0.170
2nd	0.149	0.152	0.152	0.164	0.166
3rd	0.008	0.150	0.151	0.159	0.161
4th	—	0.016	0.017	0.038	0.040
5th	—	0.004	0.004	0.006	0.006

equations (24) and (25). As a result, the relevant optimal parameters are considered herein.

Figure 13 shows the absolute acceleration transfer functions of the uncontrolled and controlled breathing mass. Shadow areas depicts the expected Band Gap regions, calculated in

the assumption of an infinite periodic metafoundation without superstructure, as explained in section 3. In the staggered-columns cases, the parameters of the unit cell were obtained by averaging their values at the first and second level. The resulting LBF and UBF are listed in table 11. All considered systems are able to reduce the breathing mass response variance, see equation (27); in addition, as expected from the analysis of PI, the transfer function peak reduces with the decreasing stiffness of the foundation outer frame; in particular, a 75% reduction with L2H3s is achieved.

Moreover, it is worthy to observe that all the LBFs listed in table 11 are close to the breathing frequency of the uncontrolled tank $\omega_b = 42.28 \text{ rad s}^{-1}$. Hence, ω_b can be taken as a reference value of LBF for the preliminary design of the foundation, so as to decrease the time required for the

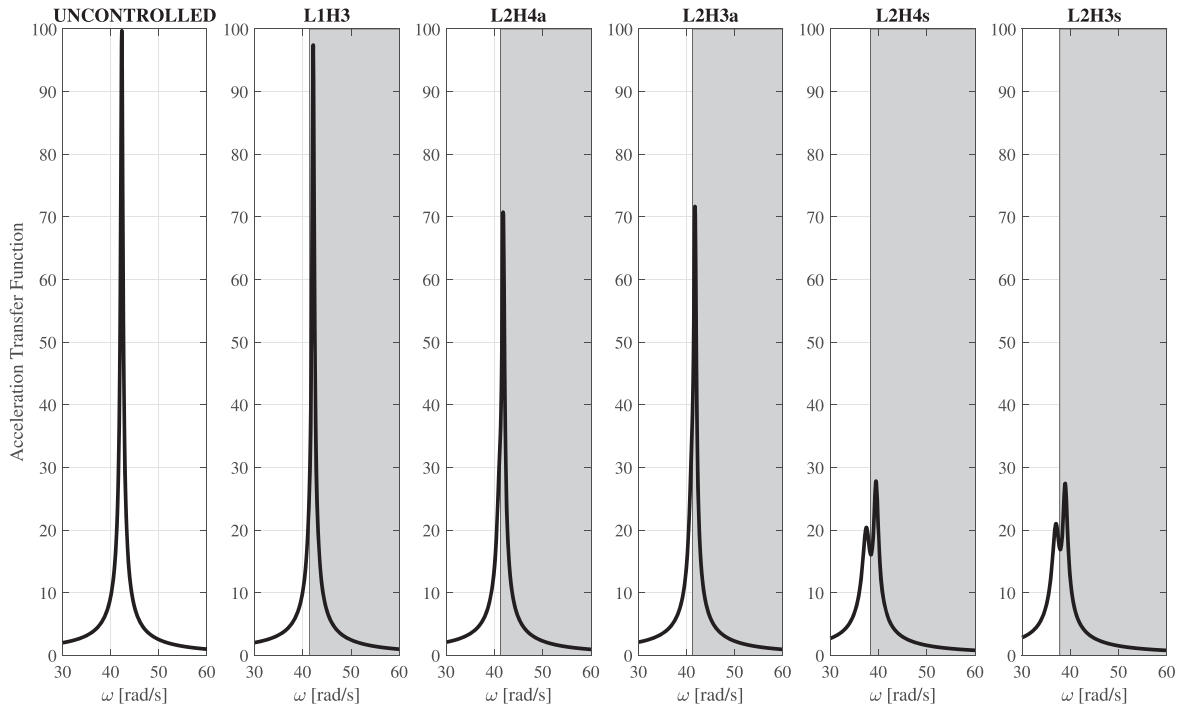


Figure 13. Breathing mass acceleration transfer functions. Shadow areas represent the expected band gap in the assumption of infinite periodic metafoundation without superstructure.

Table 11. Expected band gap limits in the assumption of infinite periodic metafoundation without superstructure.

	L1H3	L2H4a	L2H3a	L2H4s	L2H3s
LBF (rad s ⁻¹)	41.40	41.26	41.23	38.28	37.82
UBF (rad s ⁻¹)	99.17	87.74	80.78	78.15	71.02

optimization process. In this respect, previous researches, see for instance [41], showed that the LBF of locally resonant metamaterials corresponds to the resonance frequency of the resonator:

$$\text{LBF} = \sqrt{\frac{k_2}{m_2}} = \omega_2. \quad (32)$$

Therefore, in view of the vertical optimization of locally resonant metafoundations, the resonators optimal tuning frequency should be searched in an interval $\omega_2 \in [\omega_b - \Delta\omega, \omega_b + \Delta\omega]$, where $\Delta\omega$ can be safely chosen as 10 rad s^{-1} .

Eventually, in order to ascertain the feasibility of the proposed metafoundations, wire rope devices have been selected from a catalog [42] that is based on linearly elastic design values. More precisely, based on the optimal frequencies $(\omega_2)_{opt}$ of table 9 and their vertical stiffness and bearing strength properties, their number per horizontal face of each resonator, see figure 4(c), has been computed. A maximum discrepancy in terms of stiffness of 6% with respect to optimal values and an exceeding load-carrying capacity has been achieved. Relevant values are collected in table 12 and their behavior, also in agreement with section 5, is limited to the elastic regime.

5. Time history analyses

5.1. Base pressure history

In order to assess the efficacy of the proposed isolation systems when the structure is subjected to natural accelerograms, we study the time history of the hydrodynamic base pressure. To this end, EOM are solved by means of Newmark method [43], while the base pressure is calculated from equation (1).

Consider the j th accelerogram $\ddot{z}_{g,j}(t)$ and let $p_{v,j}$ be the total base pressure it entails. We define the base pressure root mean square (rms) as:

$$p_{v,j}^{\text{rms}} = \sqrt{\frac{1}{n_i} \sum_{i=1}^{N_i} |p_{v,j}(t_i)|^2}. \quad (33)$$

In this equation, t_i are the discrete points in time domain at which the accelerogram was recorded and n_i is the number of recorded points. These values are plotted against the Vertical PGA of the corresponding signals. Moreover, in order to evaluate the base pressure reduction on the wall of a controlled tank, we define an index α as ratio of the controlled rms to the uncontrolled rms:

$$\alpha_j = \frac{p_{v,c,j}^{\text{rms}}}{p_{v,u,j}^{\text{rms}}}. \quad (34)$$

A value of α_j less than 1 indicates that the metafoundation attenuated the superstructure response to the accelerogram; conversely, if α_j is greater than 1, a response amplification is pointed out.

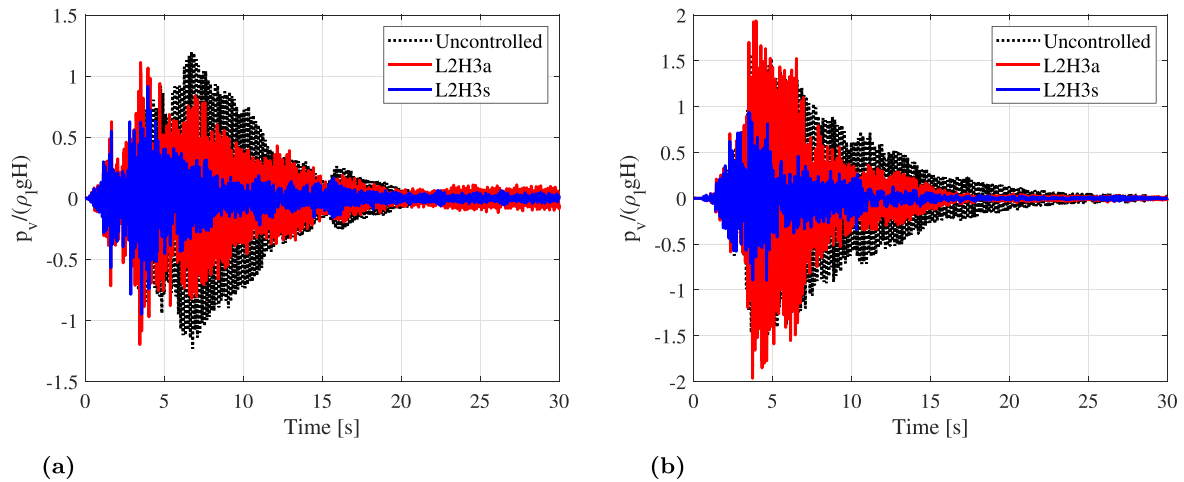


Figure 14. Comparison between the base pressure time histories for uncontrolled tank and tank isolated by means of the 3 m height two-layered foundation. (a) OBE signal Acc3; (b) SSE signal Acc12.

5.2. Results

Figure 14 shows two examples of base pressure time histories relevant to OBE and SSE accelerograms. Results of both uncontrolled tanks and tanks isolated by L2H3a and L2H3s are shown. A higher effectiveness of the staggered-columns foundation is evident.

In figure 15, the rms of the base pressure are plotted against the PGA for the foundations L2H3 -aligned and staggered-, L2H4 -aligned and staggered- and L1H3. The plots in the left column refer to OBE events while the right ones to SSE events. In order to provide better comparisons of structural responses, linear regression lines are also plotted. The aligned-column configurations present a trend of average base pressure values similar to that of the uncontrolled case. For OBE events, they reduce the response to low PGA accelerograms and exhibit a small amplification for high PGA values; for SSE events, they slightly amplify the response. The staggered-column configuration base pressures, instead, are considerably lower than the uncontrolled and aligned-columns cases thus confirming the efficacy of the proposed solution. The slopes of regression lines of SSE events are greater than those of the OBE counterparts: this highlights a stronger dependence on PGA. The single-layered foundation exhibits the same trend as the two-layered case with aligned columns, because of their similar and high outer frame stiffness.

Figure 16 depicts the RMS ratios α_j for the OBE and SSE accelerogram sets. The circular-shaped points are obtained from equation (34), while dotted lines identify each seismic record. The foundations listed on the x axis are ordered according to the vertical stiffness of the outer frame, which decreases from the left to the right. An attentive reader can notice that the staggered-columns configurations show a larger attenuation with respect to their aligned counterpart and with respect to the single-layered configuration in most of the cases (5/7 for OBE and 4/6 for SSE). In this respect, the best performance is achieved with the foundation L2H3s, with an average reduction of 22.7% for OBE signals and 23.3% for

SSE signals. Moreover, it is possible to identify some accelerograms for which the superstructure response is amplified with any type of metafoundation; the amplification is higher when the superstructure is isolated by means of a staggered-columns design. These effects are investigated herein.

5.3. Effect of the frequency content of the signals

In this subsection, we analyze the frequency content of the OBE accelerograms for which the metafoundations amplified the base pressure and we investigate its relationship with the foundations dynamic properties. Besides, we explain why the amplification was higher when the staggered-columns configurations were applied.

Figure 17(a) shows the rms ratios α for the coupled foundation-tank systems with L2H3s and L2H3a. It can be observed that the amplification occurred for the accelerograms Acc4 and Acc7. The Fourier amplitude spectra of the seven OBE earthquakes are presented in figure 17(b); in order to better analyze their frequency content, they were smoothed by means of convolution with a normalized Gaussian window. Here, we assume the frequency $\omega = 100 \text{ rad s}^{-1}$ to define a threshold between low and high frequency. Thus, the main property distinguishing Acc4 and Acc7- highlighted by red lines- from the other signals is their large frequency content in the high frequencies range.

The normalized natural modes of the considered foundations are plotted in figures 18(a), (b) for L2H3a and L2H3s, respectively. Each arrow represents the normalized modal displacement in the Z direction of the corresponding DoF, which is identified on the vertical axis. The values on the horizontal axis identify the natural circular frequencies of the two systems. Two groups of modes can be distinguished: (i) Group #1: the first three modes, whose frequency is lower than the breathing frequency ω_b of the uncontrolled tank; (ii) Group #2: modes with frequency higher than ω_b . Modes of Group #1 present a high participation of at least one local resonator, which stores the seismic energy in the form of kinetic and potential energy. Hence, it is reasonable to expect

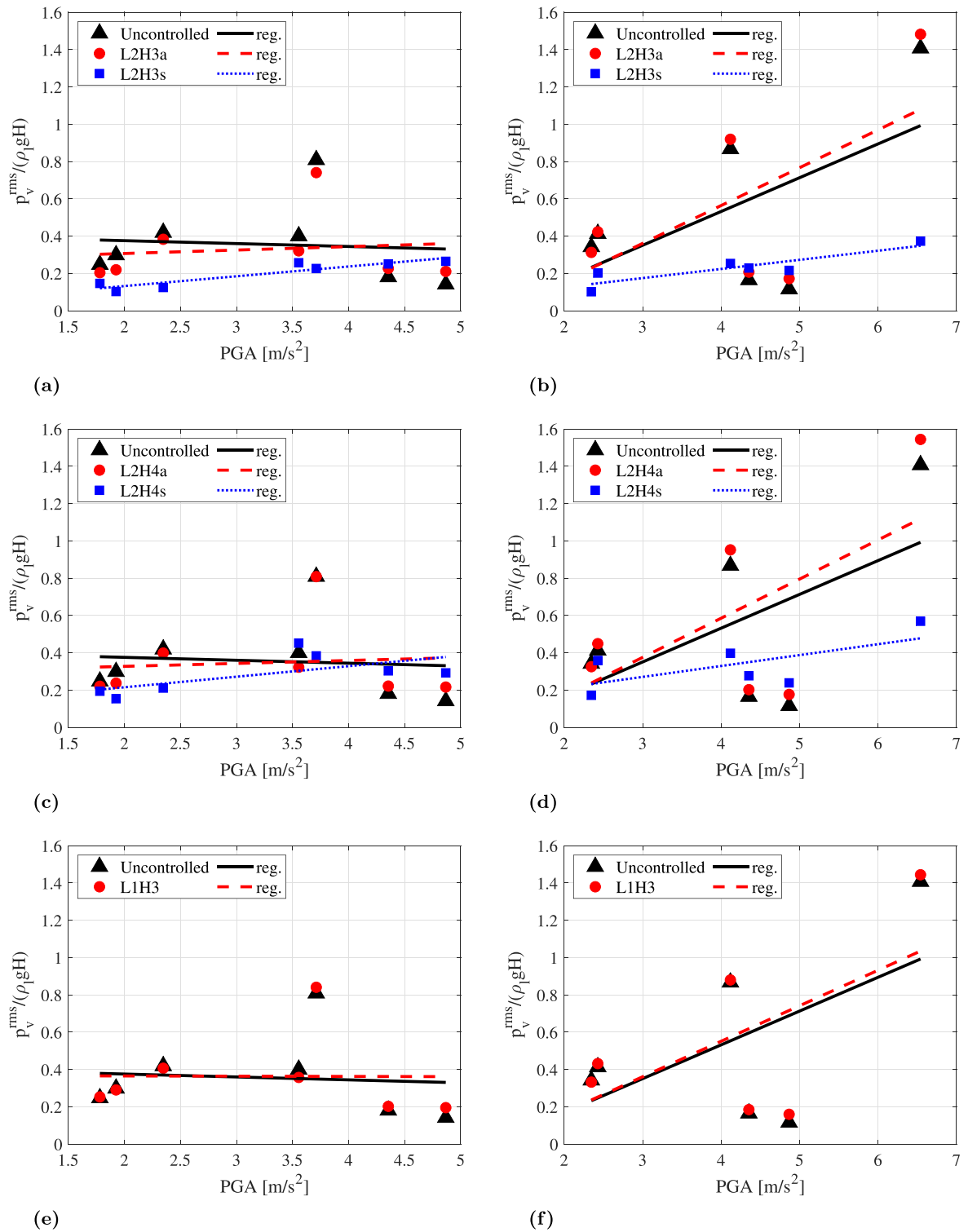


Figure 15. Base pressure RMS against PGA for uncontrolled tank and tank isolated by means of metafoundations. 3 m height two-layered foundation: (a) OBE records and (b) SSE records; 4 m height two-layered foundation: (c) OBE records and (d) SSE records; 3 m height single-layered foundation: (e) OBE records and (f) SSE records.

Table 12. Selection of type and number of wire ropes per horizontal face of resonators based on [42].

Metafoundation	L1H3	L2H4a	L2H3a	L2H4s	L2H3s
Wire rope type	WR36-400-08	WR36-200-08	WR28-400-08	WR36-600-08	WR36-600-08
Wire rope number per horizontal face of resonator	10	6	8	10	8

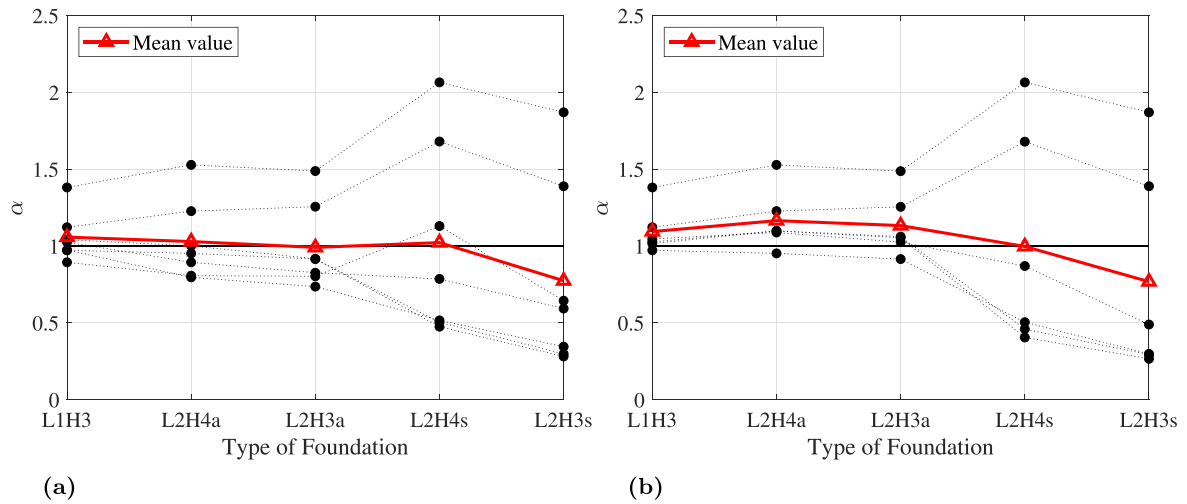


Figure 16. Base pressure rms ratios $\alpha_j = p_{v,c,j}^{\text{rms}}/p_{v,u,j}^{\text{rms}}$.

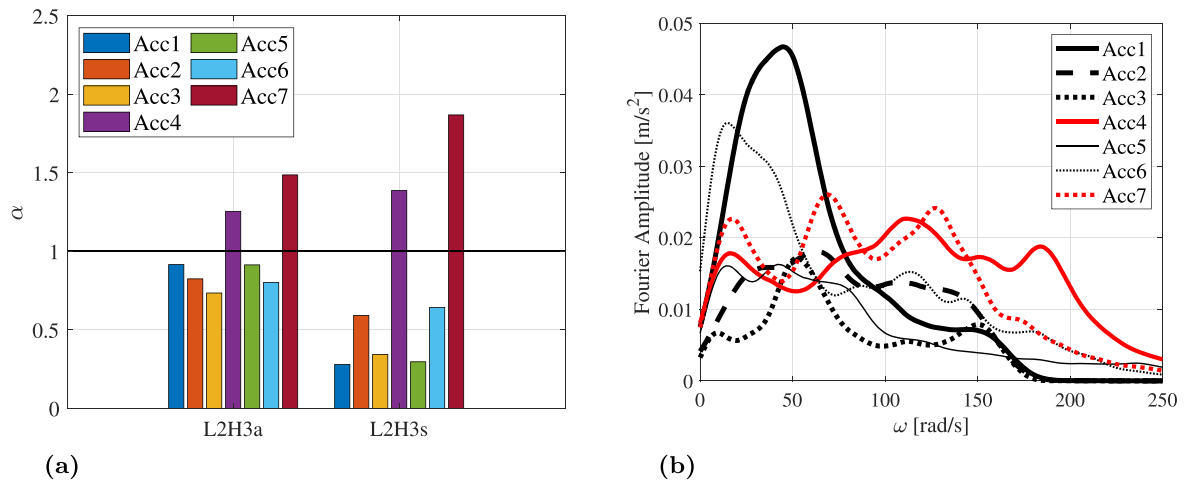


Figure 17. (a) Values of α_j for the foundations L2H3a and L2H3s; (b) amplitude spectra of OBE earthquakes.

that seismic signals with a large energy concentration in the range of Group #1 are efficiently controlled by adopting a metafoundation. For instance, the peak frequency of Acc1 amplitude spectrum is at 48 rad s^{-1} , close to the breathing frequency; nevertheless, its energy content above the 100 rad s^{-1} is low, so that the metafoundation is very efficient in reducing the hydrodynamic pressure ($\alpha = 0.28$ with L2H3s). Natural modes in Group #2 present a small normalized modal displacement of the resonators and a large participation of the two slabs. Therefore, most of the seismic energy in the range of Group #2 propagates through the foundation frame and the superstructure. Because the signals Acc4 and Acc7 exhibit a large frequency content above the 100 rad s^{-1} , the metafoundation is not efficient in controlling the hydrodynamic base pressure.

Since slabs flexural stiffness is less than columns axial stiffness, the natural frequencies of the staggered-columns configuration are lower than those of the aligned-columns configuration: we observe that the 4th natural frequency equals $373.57 \text{ rad s}^{-1}$ for L2H3a and $157.18 \text{ rad s}^{-1}$ for L2H3s. Therefore, the fourth mode of the second system lays

at a frequency range where Acc4 and Acc7 present a large energy. This mode, which belongs to Group #2, involves the highest displacement of the slab at the second level, to which the vertical impulsive mass is rigidly connected. Moreover, the breathing mass modal displacement in the fourth mode of L2H3s is higher than the one in L2H3a (0.078 versus 0.013). For these reasons, the amplification observed in the staggered-columns system subjected to Acc4 and Acc7 is higher than the corresponding amount in the aligned-columns configuration. Eventually, the same characteristics can be found by comparing the 4 m height foundations L2H4a and L2H4s.

6. Summary and conclusions

In this article, we designed feasible locally resonant metafoundations to attenuate the hydrodynamic pressure induced by vertical components of earthquakes in slender storage tanks. According to the obtained results, we draw the following conclusions: (i) metafoundations can be designed to protect slender storage tanks against vertical components of

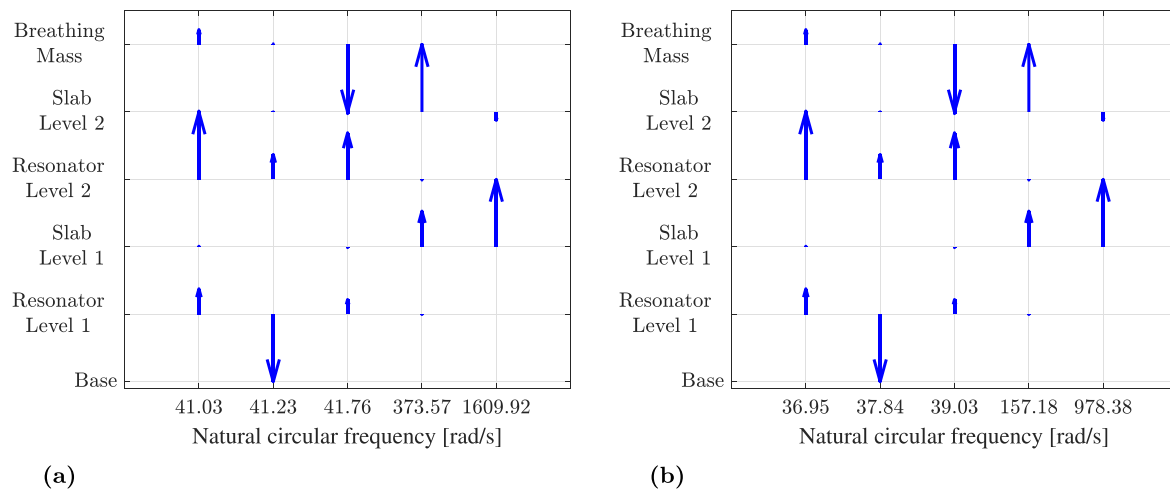


Figure 18. Natural modes and circular frequencies of the two-layered 3 m height metafoundations. (a) L2H3a; (b) L2H3s.

earthquakes; (ii) a significant performance improvement can be achieved by staggering the columns at the second level of the metafoundation frame. The best results were obtained with the 3 m height two-layered foundation L2H3s, which reduced the base pressure by 22.7% and 23.3% for OBE and SSE earthquakes, respectively; (iii) because of the high stiffness of the metafoundation outer frame in the vertical direction, the optimal parameters slightly depend on soil type; (iv) regardless of the frequency content at low frequencies, metafoundations revealed more efficient in reducing the base pressure induced by signals with a small energy content in the high frequencies range.

In-depth researches are still needed to control the response of broad tanks, in which both the breathing and the impulsive mass provide significant contributions to base pressure. Eventually, further studies are also required to experimentally characterize mechanical properties of wire ropes in the nonlinear regime and to consider more refined models for soil-structure interaction.

Acknowledgments

This work was supported by: National Natural Science Foundation of China (No. 51778488); SERA grant agreement No. 730900; the Italian Ministry of Education, University and Research (MIUR) in the frame of the ‘Departments of Excellence’ (grant L 232/2016). Moreover, the authors would like to express their gratitude to Professor Ziqi Wang—Earthquake Engineering Research and Test Center of Guangzhou University—for the useful discussion about nonstationary stochastic models of seismic records and to Professor Carlo G Lai—University of Pavia—for his indications regarding the vertical modeling of the soil.

ORCID iDs

Andrea Franchini  <https://orcid.org/0000-0001-9732-2484>
Oreste S Bursi  <https://orcid.org/0000-0003-3072-7414>

References

- [1] Yazici G and Cili F 2008 Evaluation of the liquid storage tank failures in the 1999 Kocaeli earthquake *Proceedings of the 14th World Conference on Earthquake Engineering (Beijing, China)* 12–17
- [2] Krausmann E, Renni E, Campedel M and Cozzani V 2011 Industrial accidents triggered by earthquakes, floods and lightning: lessons learned from a database analysis *Nat. Hazards* **59** 285–300
- [3] Fukasawa T, Okamura S, Somaki T, Miyagawa T, Uchita M, Yamamoto T, Watakabe T and Fujita S 2019 Research and development of three-dimensional isolation system for sodium-cooled fast reactor: Part 4 - Proposal of optimal combination method for disc spring units and newly friction model for sliding elements *American Society of Mechanical Engineers, Pressure Vessels and Piping Division (Publication) PVP8* (<https://doi.org/10.1115/PVP2019-93480>)
- [4] Marti J, Crespo M and Martínez F 2010 Seismic isolation of liquefied natural gas tanks: a comparative assessment *Seismic Isol. Protective Syst.* **1** 125–40
- [5] Veletsos A S and Tang Y 1986 Dynamics of vertically excited liquid storage tanks *J. Struct. Eng.* **112** 1228–46
- [6] Papazoglou A J and Elnashai A S 1996 Analytical and field evidence of the damaging effect of vertical earthquake ground motion *Earthq. Eng. Struct. Dyn.* **25** 1109–37
- [7] Liu Z, Zhang X, Mao Y, Zhu Y Y, Yang Z, Chan C T and Sheng P 2000 Locally resonant sonic materials *Science* **289** 1734–6
- [8] Jia G and Shi Z 2010 A new seismic isolation system and its feasibility study *Earthq. Eng. Eng. Vib.* **9** 75–82
- [9] Xiang H J, Shi Z F, Wang S J and Mo Y L 2012 Periodic materials-based vibration attenuation in layered foundations: experimental validation *Smart Mater. Struct.* **21** 112003
- [10] Shi Z and Huang J 2013 Feasibility of reducing three-dimensional wave energy by introducing periodic foundations *Soil Dyn. Earthq. Eng.* **50** 204–12
- [11] Cheng Z and Shi Z 2013 Novel composite periodic structures with attenuation zones *Eng. Struct.* **56** 1271–82
- [12] Yan Y, Laskar A, Cheng Z, Menq F, Tang Y, Mo Y L and Shi Z 2014 Seismic isolation of two dimensional periodic foundations *J. Appl. Phys.* **116**
- [13] Yan Y, Cheng Z, Menq F, Mo Y L, Tang Y and Shi Z 2015 Three dimensional periodic foundations for base seismic isolation *Smart Mater. Struct.* **24** 075006

- [14] Huang J, Shi Z, Huang W, Chen X and Zhang Z 2017 A periodic foundation with rotational oscillators for extremely low-frequency seismic isolation: analysis and experimental verification *Smart Mater. Struct.* **26** 035061
- [15] Cheng Z and Shi Z 2018 Composite periodic foundation and its application for seismic isolation *Earthq. Eng. Struct. Dyn.* **47** 925–44
- [16] Casablanca O, Ventura G, Garescì F, Azzerboni B, Chiaia B, Chiappini M and Finocchchio G 2018 Seismic isolation of buildings using composite foundations based on metamaterials *J. Appl. Phys.* **123** 174903
- [17] La Salandra V, Wenzel M, Bursi O S, Carta G and Movchan A 2017 Conception of a 3D metamaterial-based foundation for static and seismic protection of fuel storage tanks *Front. Mater.* **4** 30
- [18] Basone F, Wenzel M, Bursi O S and Fossetti M 2019 Finite locally resonant metafoundations for the seismic protection of fuel storage tanks *Earthq. Eng. Struct. Dyn.* **48** 232–52
- [19] Ministry of Infrastructure and Transport 2018 CS.LL.PP. DM 17 Gennaio, Norme tecniche per le costruzioni. Gazzetta Ufficiale della Repubblica Italiana. Building Code, in Italian
- [20] Geng Q, Zhu S and Chong K P 2018 Issues in design of one-dimensional metamaterials for seismic protection *Soil Dyn. Earthq. Eng.* **107** 264–78
- [21] Palermo A, Krödel S, Marzani A and Daraio C 2016 Engineered metabarrier as shield from seismic surface waves *Sci. Rep.* **6** 39356
- [22] Palermo A, Vitali M and Marzani A 2018 Metabarriers with multi-mass locally resonating units for broad band rayleigh waves attenuation *Soil Dyn. Earthq. Eng.* **113** 265–77
- [23] Cheng Z, Lin W and Shi Z 2018 Wave dispersion analysis of multi-story frame building structures using the periodic structure theory *Soil Dyn. Earthq. Eng.* **106** 215–30
- [24] Sun F, Xiao L and Bursi O S 2019 Optimal design and novel configuration of a locally resonant periodic foundation (lrpf) for seismic protection of fuel storage tanks *Eng. Struct.* **189** 147–56
- [25] Haroun M A and Tayel M A 1985 Response of tanks to vertical seismic excitations *Earthq. Eng. Struct. Dyn.* **13** 583–95
- [26] CEN Eurocode 8 2006 Design of structures for earthquake resistance - Part 4: Silos, tanks and pipelines *Comité Européen de Normalisation* (Brussels)
- [27] Alessandri S, Giannini R, Paolacci F and Malena M 2015 Seismic retrofitting of an HV circuit breaker using base isolation with wire ropes: I. Preliminary tests and analyses *Eng. Struct.* **98** 251–62
- [28] Alessandri S, Giannini R, Paolacci F, Amoretti M and Freddo A 2015 Seismic retrofitting of an HV circuit breaker using base isolation with wire ropes: II. Shaking-table test validation *Eng. Struct.* **98** 263–74
- [29] Balaji P S, Moussa L, Rahman M E and Vuia L T 2015 Experimental investigation on the hysteresis behavior of the wire rope isolators *J. Mech. Sci. Technol.* **29** 1527–36
- [30] Balaji P S, Leblouba M, Rahman M E and Ho L H 2016 Static lateral stiffness of wire rope isolators *Mech. Based Des. Struct. Mach.* **44** 462–75
- [31] Balaji P S, Moussa L, Rahman M E and Ho L H 2016 An analytical study on the static vertical stiffness of wire rope isolators *J. Mech. Sci. Technol.* **30** 287–95
- [32] Baker J W 2010 Conditional mean spectrum: tool for ground-motion selection *J. Struct. Eng.* **137** 322–31
- [33] ETABS, Computer & Structures, Inc., Berkeley, CA, USA (www.csiberkeley.com)
- [34] CEN Eurocode 2 2004 Design of concrete structures - Part 1-1: General rules and rules for buildings *Comité Européen de Normalisation* (Brussels)
- [35] Hu G, Tang L, Das R, Gao S and Liu H 2017 Acoustic metamaterials with coupled local resonators for broadband vibration suppression *AIP Adv.* **7** 025211
- [36] Kanai K 1957 Semiempirical formula for the seismic characteristics of the ground *Bulletin of the Earthquake Research Institute, University of Tokyo* **35** 309–25 (ci.nii.ac.jp/naid/120000866293/)
- [37] Kramer S L 1996 *Geotechnical Earthquake Engineering* (Upper Saddle River, NJ: Prentice-Hall)
- [38] C.A.R.E.C.I. 2013 *Microzonizzazione Sismica - Relazione Illustrativa: Comune di Priolo Gargallo* Università degli Studi di Messina Technical Report, in Italian (<http://www.comune.priologargallo.sr.it/wp-content/uploads/2017/06/RELAZIONE-PRIOLO-GARGALLO.pdf>)
- [39] Romano M 2011 *Relazione Geologica. Piano particolareggiato della zona di espansione CP/1. Priolo Gargallo 1603* Comune di Priolo Gargallo - Provincia di Siracusa Technical Report, in Italian (http://www.comune.priologargallo.sr.it/wp-content/uploads/old_files/public/Pubblicazione%20PRG%202015/53-Studio%20Geologico/Relazione_ZonaCP1.pdf)
- [40] Vanmarcke E H 1976 *Seismic Risk and Engineering Decisions* (Amsterdam, NL: Elsevier)
- [41] Wang G, Shao L H, Liu Y Z and Wen J H 2006 Accurate evaluation of lowest band gaps in ternary locally resonant phononic crystals *Chin. Phys.* **15** 1843–8
- [42] Wire Rope Isolator Technologies *Produced by ENIDINE* (www.enidine.com)
- [43] Chopra A K 2007 *Dynamics of Structures: Theory and Applications to Earthquake Engineering* (Prentice Hall International Series in Civil Engineering) (Upper Saddle River, NJ: Pearson/Prentice-Hall)